The Cambridge-Cambridge ROSAT Serendipity Survey -- V. Catalogue and optical identifications

Mon. Not. R. Astron. Soc. **285,** 511–528 (1997)

The Cambridge–Cambridge *ROSAT* Serendipity Survey – V. Catalogue and optical identifications

B. J. Boyle,[1]★ B. J. Wilkes[2] and M. Elvis[2]

[1]*Royal Greenwich Observatory, Madingley Road, Cambridge CB3 0EZ*
[2]*Harvard-Smithsonian Center for Astrophysics, 60 Garden St, Cambridge, MA 02138, USA*

Accepted 1996 September 18. Received 1996 July 31; in original form 1996 April 9

ABSTRACT

We report the results of a medium-depth X-ray survey of 20 *ROSAT* Position Sensitive Proportional Counter (PSPC) fields. 123 X-ray sources were detected down to a flux limit of $S(0.5\text{–}2\ \text{keV}) > 2 \times 10^{-14}$ erg s^{-1} cm^{-2} lying between that of the *Einstein* Extended Medium Sensitivity Survey (EMSS) and the deepest *ROSAT* surveys. Optical identifications of 110 of these sources have revealed 68 QSOs, 12 narrow-emission-line X-ray-luminous galaxies (NLXGs), 24 stars, two BL Lac objects, two galaxies and two clusters. CCD imaging reveals the possible presence of galaxy groups or clusters at the positions of a further four X-ray sources. The number–redshift and $\log N$–$\log S$ relations of the 68 QSOs are in better agreement with the faster rate of cosmological evolution for X-ray QSOs derived from *ROSAT* deep surveys [$L_X \propto (1+z)^{3.34 \pm 0.1}$, $z_{max} = 1.79$] than with the evolution obtained from the EMSS [$L_X \propto (1+z)^{2.55 \pm 0.1}$], the latter being rejected at greater than the 3σ level as a model for the current sample. We present the optical spectra and measurements of the emission lines. The equivalent-width distributions are consistent with those of QSO samples selected in other wavebands. We find no evidence for an inverse correlation between line width and X-ray spectral slope as recently reported for other *ROSAT* QSO samples.

Key words: surveys – galaxies: active – quasars: general – X-rays: general.

1 INTRODUCTION

The high sensitivity of the *ROSAT* Position Sensitive Proportional Counter (PSPC) has allowed a number of X-ray surveys to be made to significantly fainter flux levels than was previously possible (e.g. Shanks et al. 1991, Hasinger et al. 1993, Branduardi-Raymont et al. 1994), shedding new light on the nature of faint X-ray sources and their cosmological evolution. Results from one deep *ROSAT* survey (Boyle et al. 1994) have previously implied significantly faster QSO evolution than had been deduced from earlier surveys at somewhat higher energies, such as the *Einstein* Medium Sensitivity Survey (EMSS, Maccacaro et al. 1991). This discrepancy is not well understood: possible explanations include the different energy ranges of the *Einstein* Image Proportional Counter (IPC) (0.3–3.5 keV) and the *ROSAT* PSPC (0.5–2 keV), which can result in different spectral components dominating the QSO X-ray spectra (see Ciliegi et al. 1995, hereafter Paper III), and the inclusion of the redshift cut-off in the modelling procedure (Jones et al. 1996).

However, the EMSS and *ROSAT* deep survey also have different characteristics. This can be seen from the X-ray luminosity–redshift diagram for QSOs selected from the two samples (Fig. 1). There is little or no overlap between the distribution of QSO X-ray luminosities at a given redshift in the two surveys and thus they are sampling different parts of the QSO population. In an attempt to fill in the gap in the luminosity–redshift plane between these two surveys, we made a survey of 20 medium-depth (5000–30 000 s) PSPC observations (the Cambridge–Cambridge *ROSAT* serendipity survey, CRSS). The resulting sample, with a flux limit between the EMSS [$S(0.3\text{–}3.5\ \text{keV}) > 1 \times 10^{-13}$ erg s^{-1} cm^{-2}, Gioia et al. 1990] and the *ROSAT* deep survey [$S(0.5\text{–}2\ \text{keV}) > 4 \times 10^{-15}$ erg s^{-1} cm^{-2}, Boyle et al. 1994], results in continuous coverage of the L, z plane and overlaps with both of the other samples, facilitating a significantly improved comparison between the samples (see Fig. 1). Other X-ray samples currently near completion, e.g. the *ROSAT* International X-ray Optical Survey (RIXOS, see Page et al. 1996), will also help to fill this important gap.

★Present address: Anglo-Australian Observatory, PO Box 296, Epping, NSW 2121, Australia.

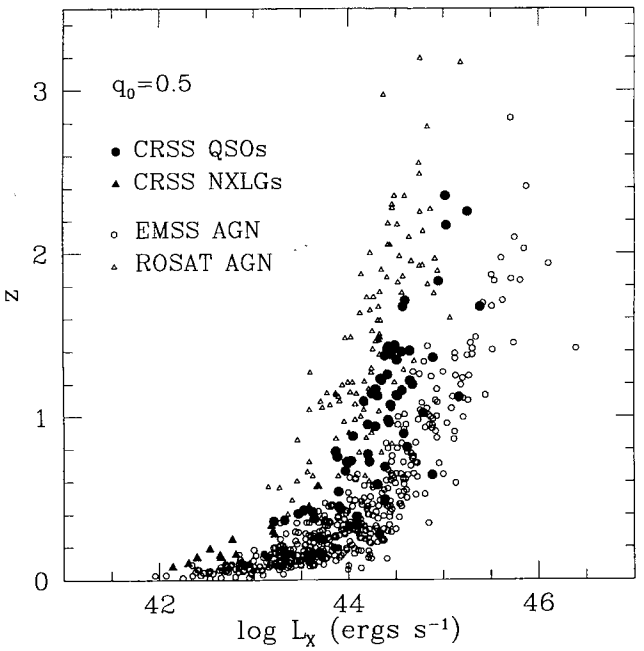

Figure 1. The coverage of the luminosity–redshift (L, z) plane afforded by the *ROSAT* deep, the *Einstein* medium (EMSS) and the current surveys.

In this paper we report the X-ray source positions and fluxes, the optical identifications and make a comparison between this survey and the EMSS and *ROSAT* deep surveys discussed above. In associated papers we also discuss the nature of the significant subset of narrow-emission-line X-ray-luminous galaxies (NLXGs) found in this sample (Boyle et al. 1995a, hereafter Paper I; Boyle et al. 1995b, hereafter Paper II), the X-ray spectral properties of the QSOs in the sample (Ciliegi et al. 1997, hereafter Paper IV), and the radio fluxes of the sample (Paper III).

2 OBSERVATIONS

2.1 X-ray source detection

ROSAT PSPC fields used in the CRSS were selected to have high Galactic latitude ($|b| > 30°$), exposure times greater than 5000 s and were available in the *ROSAT* archive prior to 1993 July. The fields were chosen to avoid bright or extended central sources which could otherwise affect the determination of the X-ray fluxes of the other sources identified in the field. To remove any remaining contribution from the central source, a central region 5 pixel in diameter on each field was excluded from any further analysis. The resulting sample included 20 fields with $14^h < \mathrm{RA} < 1^h$ and $\delta > 0°$ (Table 1). In each field source detection was limited to within 15 arcmin of the field centre in order to maintain relatively high positional accuracy for the sources (1σ error $\simeq 8$ arcsec) and to avoid obscuration by the rib support structure at larger off-axis angles.

The detection software used the IMAGES algorithm written by Dr Mike Irwin (now available as PISA in the Starlink software collection). This software counts as a significant detection any source having four or more 15-arcsec pixels with counts $\gtrsim 1.5\sigma$ above the local background level. A limiting flux level of $S(0.5\text{–}2\ \mathrm{keV}) > 2 \times 10^{-14}$ erg s^{-1} cm^{-2}, significantly greater than the faintest flux detectable for point sources even on the fields with the shortest exposures, was then applied to the source list in order to ensure completeness for all but the most extended sources in this survey. We made no attempt to discriminate between extended and point sources identified by the algorithm. Counts were then determined for each remaining source using a 5 pixel (75 arcsec) diameter circle centred on the X-ray source. The net counts in the 0.5–2 keV band ranged from 10 to 750 count for detected sources in the CRSS with a medium value of ~ 50 count.

Background subtraction was made using a single level for the whole field (typically $\sim 2.3 \times 10^{-5}$ count s^{-1} $pixel^{-1}$), determined as the median level of the background within a circle region of 15-arcmin radius centred on the field centre, after the removal of detected sources. The low background count rate results in the statistical error dominating the effects of vignetting so that no significant gradient is present. Based on a Poisson noise model, the error in the count determination is ~ 15–20 per cent at the flux limit of the survey. X-ray fluxes were determined from the net count rates of each source assuming 1 count $s^{-1} = 1.2 \times 10^{-11}$ erg cm^{-2} s^{-1}. This value is appropriate for an X-ray energy spectral slope, $\alpha_E \sim 1.3$, typical of QSOs identified in this sample (see Paper IV), and also assuming that the Galactic absorption column has negligible effect for energies > 0.5 keV. These assumptions introduce an additional uncertainty (± 10 per cent) in the reported X-ray fluxes because of the unknown spectral slope of each source.

Following the initial compilation of the catalogue, the X-ray source fluxes were subsequently revised using a much more sophisticated algorithm (see Paper IV). Full details of the X-ray flux measurement, including the source counts, background counts, hardness ratios, X-ray spectral slope and the associated errors for all the sources in the CRSS can be found in that paper.

However, for the purposes of this paper we prefer to report the original fluxes on which the initial selection of the catalogue was based. There is no significant systematic (i.e. luminosity-dependent) difference between the mean X-ray 0.5–2 keV fluxes derived by the two methods, and the rms scatter (~ 20 per cent) is consistent with the errors associated with the flux measurement for each method. We have verified that the use of the revised fluxes makes no significant difference to any of the results reported in this paper or in previous papers in this series (Papers I–II) where the original X-ray fluxes were used.

For 11 of the fields in this analysis, optical spectroscopic identification is 90 per cent complete to the X-ray flux limit. On the other fields, we subsequently imposed a brighter flux limit (listed in Table 1) to ensure a similar level of spectroscopic completeness on these fields (see Section 2.2).

A total of 123 serendipitous sources were identified in this survey. The pixel positions of each X-ray source were converted to RA, Dec. using their offset from the central 'target' source in each PSPC field (usually a QSO) the optical position of which was known to 1-arcsec accuracy.

2.2 Optical candidates

APM measurements of Palomar Observatory Sky Survey

Table 1. Survey fields.

Field Name	RA (J2000) h	m	s	Dec °	′	″	Flux Limit† ($ergs^{-1}\,cm^{-2}$)	N_H ($10^{20}\,cm^{-2}$)	ROR#	Date	PSPC	Exp.Time (sec)	# srcs†	POSS field
MKN335	00	08	19.2	20	41	24	2.0×10^{-14}	4.1	700101	1991 June 29-30	B	24586	10	EO1195
PG0027	00	30	05.7	26	17	22	2.0×10^{-14}	3.9	300016	1991 July 4-5	B	26676	7	EO1188
OQ208	14	07	00.4	28	27	14	2.0×10^{-14}	1.4	700061	1991 July 12-13	B	26050	10	EO86
PG1411	14	13	48.4	44	00	14	2.0×10^{-14}	1.2	700248	1991 June 26-27	B	25319	9	EO1386
Q1413+11	14	15	46.3	11	29	44	2.0×10^{-14}	1.8	700122	1991 July 20-21	B	28066	19	EO1051
3C298	14	19	08.2	06	28	35	2.0×10^{-13}	2.1	700865	1992 July 25-Aug 6	B	10714	1	EO1418
										1993 Jan 12	B	8884		
OQ530	14	19	46.6	54	23	14	2.0×10^{-14}	1.3	150046	1990 July 19-22	C	11516	8	EO1409
4U1417+42	14	28	32.5	42	40	25	3.0×10^{-14}	1.4	700535	1992 Jan 24	B	9593	5	EO145
PG1426	14	29	06.6	01	17	06	2.5×10^{-14}	2.7	150007	1990 July 18-19	C	6485	4	EO1440
PG1512	15	14	43.0	36	50	51	4.0×10^{-14}	1.4	700807	1992 Aug 12-17	B	5230	5	EO1610
NGC5907	15	15	52.9	56	19	33	2.0×10^{-14}	1.4	600190	1992 Jan 6-13	B	18164	9	EO1096
PG1543	15	45	30.1	48	46	12	3.0×10^{-14}	1.6	700808	1992 Aug 22-23	B	7181	5	EO1404
									700809	1992 Aug 21-22	B	5578		
MS1603.6	16	05	46.0	25	51	44	2.0×10^{-14}	4.6	300021	1991 Aug 26	B	24845	7	EO113
E1615+061	16	17	45.5	06	03	55	3.5×10^{-14}	4.6	700213	1991 Feb 19-20	B	11427	2	EO1067
3C334	16	20	21.8	17	36	22	5.0×10^{-14}	4.1	700274	1991 Mar 5-6	B	15722	1	EO55
MKN501	16	53	52.2	39	45	36	7.5×10^{-14}	1.7	700130	1991 Feb 25-26	B	7649	2	EO1135
PG1704	17	04	41.5	60	44	28	2.0×10^{-14}	2.3	700439	1991 Oct 28-30	B	13068	8	EO1414
PG2233	22	36	07.7	13	43	55	5.0×10^{-14}	4.9	700438	1991 Nov 23-24	B	6036	1	EO875
PKS2247	22	50	25.3	14	19	53	4.0×10^{-14}	4.8	700254	1991 Nov 26	B	7252	7	EO800
HR8905	23	25	22.1	23	24	13	3.0×10^{-14}	4.7	200322	1991 Jun 28-29	B	23424	3	EO843

†For which optical identification is 89 per cent complete.

(POSS) O and E plates (Irwin, Maddox & McMahon 1994) were used to generate a list of optical counterparts within 20 arcsec of each source. This radius represents 2.5 times the observed width of the X-ray to optical positional cross-correlation function [see fig. 1(a) in Paper I]. 112 of the 123 X-ray sources (91 per cent) had at least one optical counterpart within this range to the limit of the POSS plates ($O<22$ mag, $E<20$ mag). The typical error in the optical magnitudes determined from the POSS plates is ±0.2 mag (Irwin et al. 1994). The mean $O-E$ colour of these counterparts is much bluer than the overall colour distribution [see fig. 1(b) in Paper I], demonstrating that the counterparts are, as expected, dominated by QSOs ($O-E\sim1$ mag, McMahon 1991). The X-ray source positions were subsequently revised to give a zero mean positional offset in each field between the X-ray and optical positions of sources with a blue ($O-E<1.2$ mag) optical counterpart. This correction changed the nearest optical counterpart in 5 per cent of the total sample. The revised X-ray positions for all 123 sources are given in Table 2. The 0.5–2 keV fluxes for

Table 2. Optical identifications.

Survey Name	$S_{0.5-2keV}$	X-ray RA (J2000) h	m	s	Dec °	′	″	θ	Optical RA (J2000) h	m	s	Dec °	′	″	O–X	E	O	ID	z	Notes
	$ergs^{-1}\,cm^{-2}$							′							″					
CRSS0007.3+2042	0.48×10^{-13}	00	07	21.9	+20	42	04	13.6	00	07	21.7	+20	42	02	2.6	18.53	18.78	QSO	0.769	
CRSS0007.5+2034	0.34×10^{-13}	00	07	33.4	+20	34	46	12.7	00	07	33.8	+20	34	39	9.1	15.29	17.81	M(e)		
CRSS0007.7+2050	0.29×10^{-13}	00	07	43.0	+20	50	39	12.2	00	07	42.7	+20	50	39	4.0*	–	20.76	QSO	1.396	
CRSS0008.0+2043	0.23×10^{-13}	00	08	02.0	+20	43	56	4.9	00	08	02.4	+20	44	11	16.8	17.68	17.93	QSO	1.381	
CRSS0008.4+2034	0.16×10^{-12}	00	08	26.4	+20	34	34	7.6	00	08	26.5	+20	34	32	1.8*	16.34	16.84	QSO	0.389	
CRSS0008.4+2042	0.20×10^{-13}	00	08	09.3	+20	42	10	2.2	00	08	29.5	+20	42	00	9.6*	19.28	19.85	QSO	1.710	
CRSS0008.4+2035	0.24×10^{-13}	00	08	29.7	+20	34	01	7.8	00	08	29.8	+20	34	00	1.9	18.25	21.41	M		
CRSS0008.6+2045	0.24×10^{-13}	00	08	40.6	+20	45	57	6.6	00	08	40.9	+20	46	00	5.1	–	20.72	QSO	0.752	
CRSS0008.9+2050	0.68×10^{-12}	00	08	54.0	+20	50	26	11.7	00	08	54.1	+20	50	36	10.5*	11.26	14.83	M(e)		
CRSS0009.0+2041	0.20×10^{-13}	00	09	01.3	+20	41	33	9.7	00	09	01.7	+20	41	35	6.6*	19.04	21.83	NLXG	0.190	HII[1]
CRSS0029.1+2616	0.34×10^{-13}	00	29	07.5	+26	16	22	13.2	No optical counterpart on POSS									Group		CCD[2]
CRSS0029.7+2606	0.20×10^{-13}	00	29	44.7	+26	06	37	11.9	00	29	44.0	+26	06	27	13.8	18.88	19.26	QSO	1.094	
CRSS0030.2+2611	0.51×10^{-13}	00	30	17.3	+26	11	43	6.4	00	30	17.4	+26	11	38	4.9	14.84	16.26	NLXG	0.077	HII[1]
CRSS0030.5+2618	0.15×10^{-12}	00	30	33.4	+26	18	16	6.2	00	30	34.0	+26	18	08	11.1†	19.44	–	Gal	0.516	Cluster[2]
									00	30	33.3	26	18	10	5.9*	19.75	–	Gal?	0.52?	
CRSS0030.6+2620	0.19×10^{-12}	00	30	39.5	+26	20	53	8.1	00	30	39.6	+26	20	54	1.7*	16.87	17.31	QSO	0.493	
CRSS0030.7+2616	0.20×10^{-13}	00	30	47.2	+26	16	50	9.3	00	30	47.9	+26	16	47	9.4	18.45	–	NLXG	0.247	Sy2[1]
CRSS0030.8+2628	0.20×10^{-13}	00	30	48.7	+26	28	26	13.9	00	30	48.8	+26	28	31	5.7	19.15	19.64	QSO	1.372	
CRSS1406.2+2830	0.65×10^{-13}	14	06	16.2	+28	30	50	10.3	14	06	15.6	+28	30	52	8.8*	19.66	–	Gal	0.546	
CRSS1406.7+2827	0.25×10^{-13}	14	06	44.3	+28	27	21	3.5	14	06	44.3	+28	27	25	4.7	–	20.57	QSO	0.878	
CRSS1406.7+2838	0.28×10^{-13}	14	06	47.3	+28	38	54	11.9	14	06	48.0	+28	38	53	8.9	–	22.10	NLXG	0.331	HII[1]
CRSS1406.9+2834	0.15×10^{-12}	14	06	54.3	+28	34	14	6.7	14	06	54.0	+28	34	17	4.3*	12.77	16.73	Gal	0.118	Cluster[4]
									14	06	53.8	+28	34	08	9.0*	–	21.49	Gal	0.118	
CRSS1407.3+2818	0.19×10^{-12}	14	07	19.4	+28	18	11	10.3	14	07	19.4	+28	18	14	2.8	17.23	17.76	QSO	1.121	
CRSS1407.3+2814	0.36×10^{-13}	14	07	20.3	+28	14	56	13.2	14	07	20.2	+28	14	50	6.4†	16.88	18.00	QSO	0.728	[5]
									14	07	20.5	+28	14	58	2.6*	–	21.42	?		
CRSS1407.6+2825	0.24×10^{-13}	14	07	38.9	+28	25	12	8.9	14	07	38.4	+28	25	15	6.8	18.95	19.73	QSO	1.222	

Table 2 – *continued*

Survey Name	X-ray $S_{0.5-2\,keV}$ erg s^{-1} cm^{-2}	X-ray RA (J2000) h m s	X-ray Dec ° ′ ″	θ ′	Optical RA (J2000) h m s	Optical Dec ° ′ ″	O-X ″	E	O	ID	z	Notes
CRSS1407.7+2830	0.34×10^{-12}	14 07 45.2	+28 30 24	10.3	14 07 45.4	+28 30 28	4.8*	18.40	18.81	QSO	0.642	
CRSS1407.7+2824	0.42×10^{-13}	14 07 45.6	+28 24 33	10.6	14 07 45.3	+28 24 35	4.0	–	21.49	QSO	1.127	
CRSS1407.8+2833	0.35×10^{-13}	14 07 51.7	+28 33 14	12.7	14 07 50.8	+28 33 21	14.3*	–	21.96	N/O		
					14 07 51.7	+28 33 31	16.3*	–	22.09	N/O		
CRSS1412.5+4355	0.22×10^{-12}	14 12 31.6	+43 55 41	14.7	14 12 31.6	+43 55 35	5.1*	15.86	17.03	NLXG	0.095	Sy1.8[1]
CRSS1413.0+4406	0.28×10^{-13}	14 13 04.3	+44 06 59	9.8	No optical counterpart on POSS					Group		CCD[6]
CRSS1413.3+4405	0.52×10^{-13}	14 13 20.0	+44 05 31	7.0	14 13 19.9	+44 05 35	4.6	17.19	–	NLXG	0.136	Sy1.5[1]
CRSS1413.4+4358	0.30×10^{-13}	14 13 28.8	+43 58 06	4.1	14 13 28.9	+43 58 07	1.7*	19.81	20.19	QSO	0.950	
CRSS1413.8+4406	0.46×10^{-13}	14 13 48.4	+44 06 43	5.9	14 13 48.3	+44 06 46	3.7*	19.06	–	QSO	0.978	
CRSS1413.8+4402	0.28×10^{-13}	14 13 53.1	+44 02 27	2.1	14 13 53.0	+44 02 30	3.9*	19.58	–	QSO	1.347	
CRSS1413.9+4352	0.43×10^{-13}	14 13 59.6	+43 52 06	8.4	No optical counterpart on POSS					?		CCD[7]
CRSS1414.2+4354	0.53×10^{-13}	14 14 14.3	+43 54 16	7.7	14 14 14.2	+43 54 14	1.9*	19.09	19.72	QSO	1.197	
CRSS1415.0+4402	0.29×10^{-13}	14 14 59.5	+44 02 10	13.0	14 15 00.2	+44 02 11	8.0*	17.60	–	NLXG	0.136	Sy1.5[1]
CRSS1415.0+1119	0.51×10^{-13}	14 15 04.8	+11 19 39	14.8	14 15 04.6	+11 19 41	3.6	19.03	20.06	QSO	0.538	
CRSS1415.1+1140	0.26×10^{-13}	14 15 11.1	+11 40 01	12.6	14 15 11.2	+11 40 03	2.7*	19.36	19.87	QSO	2.353	
CRSS1415.2+1123	0.23×10^{-13}	14 15 15.7	+11 23 44	10.1	14 15 15.9	+11 23 44	2.6*	19.17	19.93	QSO	1.230	
CRSS1415.2+1119	0.61×10^{-13}	14 15 16.6	+11 19 34	13.0	14 15 17.5	+11 19 21	18.7	16.87	18.16	G		[8]
CRSS1415.3+1137	0.46×10^{-13}	14 15 23.7	+11 37 38	9.1	No optical counterpart on POSS					?		CCD[9]
CRSS1415.5+1127	0.20×10^{-13}	14 15 30.9	+11 27 11	4.7	14 15 31.1	+11 27 13	3.6*	–	21.51	QSO	1.412	
CRSS1415.5+1131	0.15×10^{-12}	14 15 31.5	+11 32 00	3.8	14 15 31.5	+11 31 57	3.5*	18.38	19.91	QSO	0.257	
CRSS1415.5+1128	0.25×10^{-13}	14 15 32.1	+11 28 53	3.9	14 15 32.0	+11 28 50	3.4	19.74	21.79	QSO	0.360	
CRSS1415.6+1127	0.41×10^{-13}	14 15 38.0	+11 27 46	3.4	No optical counterpart on POSS					?		CCD[10]
CRSS1415.6+1124	0.62×10^{-13}	14 15 39.8	+11 24 12	6.0	14 15 40.1	+11 24 03	10.1*	17.59	–	M(e)		
CRSS1415.7+1116	0.26×10^{-13}	14 15 44.5	+11 16 29	13.7	14 15 44.4	+11 16 26	2.5*	18.84	19.19	QSO	1.257	
CRSS1415.9+1139	0.34×10^{-13}	14 15 56.5	+11 39 09	9.6	No optical counterpart on POSS					?		CCD[11]
CRSS1416.0+1142	0.40×10^{-13}	14 16 02.2	+11 42 45	12.9	No optical counterpart on POSS					?		CCD[12]
CRSS1416.2+1136	0.52×10^{-13}	14 16 12.6	+11 36 17	9.0	14 16 13.1	+11 36 07	12.4	19.50	22.22	?		
CRSS1416.2+1131	0.20×10^{-13}	14 16 15.4	+11 31 10	7.3	14 16 15.9	+11 31 09	7.2	–	21.69	QSO	1.429	
CRSS1416.3+1129	0.22×10^{-13}	14 16 19.5	+11 29 53	8.2	No optical counterpart on POSS					Group		CCD[13]
CRSS1416.3+1137	0.21×10^{-13}	14 16 21.0	+11 37 53	11.2	14 16 20.7	+11 37 37	15.3	19.28	20.77	BL		[14]
CRSS1416.3+1124	0.20×10^{-13}	14 16 23.0	+11 24 42	10.7	14 16 23.5	+11 24 40	7.4*	–	20.95	QSO	1.673	BAL
CRSS1416.3+1140	0.52×10^{-13}	14 16 23.7	+11 40 21	13.8	14 16 23.5	+11 40 27	6.7*	17.37	18.57	G		[15]
CRSS1418.3+0637	0.19×10^{-12}	14 18 20.9	+06 37 49	14.6	14 18 21.3	+06 37 46	6.4*	16.91	17.41	QSO	0.329	
CRSS1419.2+5429	0.33×10^{-13}	14 19 16.1	+54 29 32	7.4	14 19 16.2	+54 29 42	10.2	19.29	19.90	QSO	0.722	
CRSS1419.2+5414	0.50×10^{-13}	14 19 16.7	+54 14 17	9.9	14 19 17.1	+54 14 16	3.3*	16.67	19.55	Gal	0.226	
CRSS1419.3+5424	0.21×10^{-13}	14 19 18.3	+54 24 31	4.2	14 19 19.0	+54 24 33	5.8*	19.81	20.45	QSO	0.785	
CRSS1419.5+5428	0.27×10^{-13}	14 19 32.6	+54 28 21	5.4	14 19 31.8	+54 28 19	7.7*	15.27	17.05	G		[16]
					14 19 32.6	54 28 12	8.4*	–	21.65	?		
CRSS1419.8+5433	0.31×10^{-13}	14 19 51.6	+54 33 57	10.1	14 19 52.6	+54 33 55	8.6*	19.52	21.31	QSO	0.367	
CRSS1419.8+5419	0.27×10^{-13}	14 19 53.3	+54 19 25	4.1	14 19 53.8	+54 19 20	6.1	11.06	12.44	N/O		Bright Star
CRSS1419.9+5430	0.49×10^{-13}	14 19 54.9	+54 30 18	7.2	14 19 54.1	+54 30 14	7.9	17.45	17.93	QSO	2.257	
CRSS1420.1+5426	0.11×10^{-12}	14 20 09.2	+54 26 38	4.5	14 20 09.4	+54 26 38	2.1	19.03	20.24	QSO	0.583	
CRSS1428.0+4244	0.32×10^{-13}	14 27 59.8	+42 44 15	6.9	14 28 00.2	+42 44 10	6.8	15.07	17.62	M(e)		
CRSS1428.3+4231	0.32×10^{-13}	14 28 20.3	+42 31 34	10.0	14 28 20.4	+42 31 38	3.8*	17.72	18.27	QSO	2.171	
CRSS1429.0+0122	0.47×10^{-13}	14 29 04.5	+01 22 29	4.4	14 29 04.4	+01 22 30	2.3*	19.19	20.00	QSO	0.416	
CRSS1429.0+0120	0.43×10^{-13}	14 29 04.7	+01 20 29	2.5	14 29 04.7	+01 20 17	11.9†	16.56	18.26	NLXG	0.102	HII[1,17]
					14 29 05.1	+01 20 32	6.8*	16.78	17.95	F		
CRSS1429.1+0128	0.41×10^{-13}	14 29 11.8	+01 28 09	10.5	14 29 11.8	+01 28 00	9.3	–	21.35	QSO	1.131	
CRSS1429.2+0120	0.26×10^{-13}	14 29 17.9	+01 20 56	4.4	14 29 17.7	+01 21 00	4.7	18.18	18.95	QSO	1.127	
CRSS1429.0+4230	0.89×10^{-13}	14 29 01.5	+42 30 53	11.0	14 29 01.8	+42 30 54	3.1	9.90	11.16	F		
CRSS1429.1+4241	0.62×10^{-13}	14 29 06.4	+42 41 10	6.2	No optical counterpart on POSS					Group		CCD[18]
CRSS1429.7+4240	0.13×10^{-12}	14 29 45.1	+42 40 58	13.3	14 29 45.1	+42 40 54	4.0	15.25	16.87	QSO	1.672	
CRSS1514.3+5621	0.50×10^{-12}	15 14 22.9	+56 21 29	12.8	15 14 22.9	+56 21 33	3.5*	13.91	16.09	M(e)		
CRSS1514.4+5627	0.37×10^{-13}	15 14 30.0	+56 26 59	14.0	15 14 29.6	+56 27 07	8.9	–	20.69	NLXG	0.446	
CRSS1514.7+3641	0.48×10^{-13}	15 14 47.1	+36 41 50	9.9	15 14 47.0	+36 41 50	1.4	19.02	20.08	QSO	1.219	
CRSS1515.0+3649	0.18×10^{-12}	15 15 03.5	+36 49 48	4.5	15 15 03.4	+36 49 50	2.2	7.66	8.30	N/O		Bright Star
CRSS1515.0+3657	0.16×10^{-12}	15 15 05.0	+36 57 26	7.5	15 15 05.0	+36 57 21	4.0	19.41	20.47	QSO	0.253	
CRSS1515.1+5628	0.57×10^{-13}	15 15 10.2	+56 28 30	10.6	15 15 10.1	+56 28 34	4.7	–	20.06	QSO	0.723	
CRSS1515.4+3652	0.82×10^{-13}	15 15 26.8	+36 51 56	8.7	15 15 26.7	+36 52 03	7.3*	19.98	20.68	QSO	0.893	
CRSS1515.5+3655	0.11×10^{-12}	15 15 35.2	+36 55 54	11.2	15 15 35.4	+36 55 49	5.2*	18.72	19.53	QSO	0.812	
CRSS1515.7+5610	0.37×10^{-13}	15 15 47.1	+56 10 32	9.4	15 15 47.5	+56 10 33	3.3	19.25	20.29	QSO	0.296	
CRSS1516.3+5611	0.23×10^{-13}	15 16 22.1	+56 11 53	9.1	15 16 22.0	+56 11 50	2.7*	–	20.59	QSO	1.168	
CRSS1516.4+5612	0.25×10^{-13}	15 16 26.2	+56 12 46	8.5	15 16 26.0	+56 12 50	4.0	–	21.61	M		
CRSS1516.8+5617	0.32×10^{-13}	15 16 53.4	+56 17 45	8.5	No optical counterpart on POSS					?		CCD[19]
CRSS1517.0+5623	0.85×10^{-13}	15 17 03.8	+56 23 40	10.3	15 17 03.6	+56 23 38	2.1*	19.36	20.38	QSO	0.434	
CRSS1517.6+5619	0.80×10^{-13}	15 17 39.6	+56 19 24	14.6	15 17 39.4	+56 19 15	8.9	13.99	15.50	G		
CRSS1545.4+4838	0.37×10^{-13}	15 45 26.4	+48 38 27	8.5	15 45 26.5	+48 38 21	6.5*	–	20.94	QSO	0.937	
CRSS1545.5+4858	0.38×10^{-13}	15 45 34.6	+48 58 13	11.5	15 45 34.6	+48 58 16	3.2*	19.39	19.54	QSO	0.666	
CRSS1545.5+4847	0.35×10^{-13}	15 45 36.1	+48 47 19	1.1	15 45 35.9	+48 47 13	6.3	18.85	19.93	QSO	1.403	
CRSS1545.9+4849	0.58×10^{-13}	15 45 55.7	+48 49 37	4.9	15 45 55.6	+48 49 29	8.1*	18.68	20.93	QSO	0.154	
CRSS1546.4+4849	0.32×10^{-13}	15 46 25.3	+48 49 53	9.7	15 46 25.4	+48 49 58	5.0	18.84	19.99	F		[20]
CRSS1604.8+2549	0.36×10^{-13}	16 04 51.8	+25 49 58	12.2	16 04 51.9	+25 49 58	2.0	19.78	20.96	QSO	0.426	

Table 2 – *continued*

Survey Name	$S_{0.5-2\,keV}$	X-ray RA (J2000)	Dec	θ	Optical RA (J2000)	Dec	O-X	E	O	ID	z	Notes
	erg s^{-1} cm^{-2}	h m s	° ′ ″	′	h m s	° ′ ″	″					
CRSS1604.9+2545	0.38×10^{-13}	16 04 56.0	+25 45 26	13.1	16 04 55.7	+25 45 20	6.9	16.44	17.51	G		
CRSS1605.2+2602	0.28×10^{-13}	16 05 12.8	+26 02 42	12.6	No optical counterpart on POSS					?		CCD[21]
CRSS1605.2+2541	0.40×10^{-13}	16 05 17.0	+25 41 17	12.6	16 05 17.2	+25 41 19	3.4*	18.47	18.88	QSO	1.071	
CRSS1605.6+2543	0.44×10^{-13}	16 05 39.8	+25 43 10	8.9	16 05 39.9	+25 43 10	1.8	18.93	20.21	NLXG	0.278	HII[1]
CRSS1605.9+2554	0.41×10^{-13}	16 05 58.5	+25 54 05	3.7	16 05 58.7	+25 54 07	3.5*	–	20.55	NLXG	0.151	
CRSS1606.6+2542	0.23×10^{-13}	16 06 35.9	+25 42 41	14.9	16 06 36.1	+25 42 45	4.1*	18.53	19.03	QSO	1.436	
CRSS1618.0+0617	0.18×10^{-12}	16 18 04.6	+06 17 17	13.7	16 18 04.7	+06 17 07	9.7*	13.62	15.74	M(e)		
CRSS1618.4+0558	0.35×10^{-13}	16 18 26.6	+05 58 22	12.0	16 18 27.3	+05 58 15	12.7*	19.29	20.45	QSO	0.406	
CRSS1620.1+1724	0.65×10^{-12}	16 20 11.3	+17 24 28	12.7	16 20 11.3	+17 24 27	1.2*	15.21	15.67	QSO	0.114	PG1617+175[22]
CRSS1653.3+3951	0.91×10^{-13}	16 53 23.8	+39 51 21	7.8	16 53 23.7	+39 51 24	3.1	–	20.50	QSO	0.692	
CRSS1654.5+3954	0.21×10^{-12}	16 54 30.8	+39 54 21	11.3	16 54 30.8	+39 54 20	0.8*	18.49	19.23	QSO	0.340	
CRSS1703.9+6045	0.10×10^{-12}	17 03 55.6	+60 45 08	5.6	17 03 55.7	+60 45 11	2.7	17.81	19.69	QSO	0.284	MS1703.2+6049[23]
CRSS1704.1+6047	0.66×10^{-13}	17 04 05.9	+60 47 49	5.0	17 04 06.1	+60 47 53	4.6*	17.25	18.12	QSO	1.362	
CRSS1704.6+6036	0.23×10^{-13}	17 04 39.7	+60 36 54	8.5	17 04 39.0	+60 36 49	7.7	18.50	21.35	M		
CRSS1705.3+6049	0.27×10^{-13}	17 05 17.8	+60 49 53	6.4	17 05 18.3	+60 49 54	3.7	19.95	21.83	NLXG	0.572	Sy2?[1]
CRSS1705.3+6044	0.24×10^{-13}	17 05 22.9	+60 44 55	5.1	17 05 23.7	+60 44 57	6.0*	18.79	19.29	QSO	1.416	
CRSS1705.4+6031	0.61×10^{-13}	17 05 27.2	+60 31 10	14.5	17 05 26.4	+60 31 03	9.7*	17.22	18.19	QSO	0.375	
CRSS1705.5+6042	0.55×10^{-12}	17 05 34.9	+60 42 16	7.0	17 05 34.7	+60 42 15	1.6	18.09	20.36	BL	0.280	MS1704.9+6046[23]
CRSS1706.4+6042	0.22×10^{-13}	17 06 26.2	+60 42 59	13.1	17 06 26.6	+60 42 45	14.3†	18.05	18.74	QSO	1.142	[24]
					17 06 26.0	+60 43 01	2.9*	19.39	21.24	N/O		
					17 06 27.5	+60 42 55	10.0*	18.14	20.17	N/O		
CRSS2235.3+1340	0.98×10^{-13}	22 35 18.2	+13 40 09	12.8	22 35 18.3	+13 40 07	2.4*	19.22	19.89	QSO	1.021	Q2232+134[25]
CRSS2249.5+1425	0.34×10^{-12}	22 49 30.5	+14 25 11	14.2	22 49 30.5	+14 25 09	1.5*	11.93	13.16	F		
CRSS2250.0+1407	0.44×10^{-13}	22 50 01.2	+14 07 34	14.2	22 50 01.2	+14 07 40	5.4*	19.83	20.92	QSO	1.159	
CRSS2250.1+1414	0.94×10^{-13}	22 50 06.6	+14 14 58	6.7	22 50 06.3	+14 14 54	6.4	10.57	11.43	F		
CRSS2250.4+1431	0.79×10^{-12}	22 50 24.1	+14 31 43	11.1	22 50 24.2	+14 31 44	1.7	11.71	13.65	G		
CRSS2250.8+1429	0.47×10^{-13}	22 50 51.2	+14 29 23	11.1	22 50 51.4	+14 29 29	6.8	15.83	17.93	M(e)		
CRSS2250.9+1419	0.34×10^{-13}	22 50 59.5	+14 19 20	8.3	22 50 59.5	+14 19 20	0.7	16.71	19.32	M(e)		
CRSS2251.0+1418	0.49×10^{-13}	22 51 01.6	+14 18 32	9.0	22 51 01.8	+14 18 26	6.1	18.54	19.02	QSO	0.962	
CRSS2324.7+2315	0.39×10^{-13}	23 24 43.1	+23 15 37	12.5	23 24 43.8	+23 15 37	9.3	18.55	18.98	QSO	1.828	
CRSS2324.8+2321	0.77×10^{-13}	23 24 49.9	+23 21 02	8.3	23 24 50.5	+23 21 06	9.6	19.14	19.68	QSO	0.447	
CRSS2325.1+2330	0.45×10^{-13}	23 25 09.2	+23 30 14	6.0	23 25 09.6	+23 30 16	6.1	10.56	12.63	F		

Notes to the table.

N/O: not observed spectroscopically.

*More than one optical counterpart within 20 arcsec of the X-ray position.

†True optical counterpart is not the closest object.

[1]Detailed identification from Boyle et al. (1995b).

[2]The galaxy excess within 20 arcsec of X-ray source is just over twice that of the background.

[3]Optical spectra of both objects are consistent with $z=0.52$ galaxies, although the spectrum of the galaxy closer to the X-ray source position has a low signal-to-noise ratio. The CCD image indicates the presence of a rich cluster.

[4]Galaxy cluster on the Palomar sky survey plate.

[5]The closest optical counterpart is a faint source with an ambiguous optical spectrum. However, the most likely identification of the X-ray source in the QSO 6 arcsec from the X-ray position.

[6]A group of six galaxies is seen within 20 arcsec of the X-ray source position.

[7]There are three galaxies within 20 arcsec of the X-ray source position, including an $R\sim20$ galaxy located at the centre of the X-ray error circle. However, the numbers of galaxies found do not quite exceed the criterion for acceptance of a group.

[8] The a posteriori probability of finding an optical counterpart of this magnitude or brigher within a 20-arcsec radius is ~0.02. It is therefore possible that this star is not the correct counterpart of the X-ray source, but it is the only object identified within the 20-arcsec error radius down to the photographic plate limit.

[9]There is a single galaxy at the X-ray source position, but no obvious cluster.

[10]There are six faint galaxies within 20 arcsec of the X-ray source position, but the field does not quite meet the criterion for acceptance as a group.

[11]Only one faint galaxy is seen within 20 arcsec of the X-ray source position.

[12]Not classified as a group, but there is a compact group of five galaxies, centred within 20 arcsec of the X-ray source position.

[13]There are eight faint galaxies within 20 arcsec of the X-ray source position.

[14]Continuum object.

[15]The a posteriori probability of finding an object of this magnitude or brighter within a 20-arcsec radius is ~0.03. It is therefore possible that this star is not the correct counterpart of the X-ray source. However, the only other optical source within the error circle is a faint $E=19.7$ galaxy, 18 arcsec from the X-ray source position.

[16]Although the probability of finding such a bright star within the error radius is very low <0.01, a second (almost equidistant) faint candidate was observed spectroscopicaly, but no strong emission lines were found.

[17]Although an F star was found to be closer to the X-ray source position, the low probability of identifying a starburst galaxy within 12 arcsec makes it the more probable X-ray source counterpart.

[18]There are five faint galaxies within 20 arcsec of the X-ray source position.

[19]There are three faint galaxies within 20 arcsec, but no obvious group.

[20]The a posteriori probability of finding a star of this magnitude or brighter within a 20-arcsec radius is ~0.05. It is therefore possible that this is not the true counterpart of the X-ray source, but there are no other objects within 20 arcsec visible on the POSS plates.

[21]No obvious group within 20 arcsec of the X-ray source position.

[22]Optical identification and redshift from Schmidt & Green (1983).

[23]Optical identification and redshift from Stocke et al. (1991).

[24]The QSO observed is not the closest object to the X-ray source position. Two faint objects were found closer to the X-ray position but were not observed.

[25]Optical identification and redshift from Crampton, Cowley & Hartwick (1987).

these sources and PSPC off-axis angle in arcmin (θ) are also given in this table, together with the optical positions, O and E magnitudes, and the optical-to-X-ray positional offset in arcsec ($O-X$) for all the optical counterparts with spectroscopic identifications. The survey names were derived from the J2000 optical positions, X-ray positions were used when no optical identification was available.

2.3 Optical spectroscopy

Low-resolution (3 Å pixel^{-1}) spectroscopy was obtained for the optical counterparts with the ISIS double arm spectrograph at the William Herschel Telescope (WHT) on the nights of 1993 June 19–20. ISIS was operated with 158 line mm^{-1} gratings in the blue and red arms (a dichroic filter was used to split the light at 5400 Å), with the Tektronix and EEV CCDs as the detectors in the blue and red arms respectively.

Throughout the run the seeing was ~ 1 arcsec, and most of the observations were made with a 1.5-arcsec slit positioned at the parallactic angle. In these conditions, exposure times of 300–2400 s were sufficient to yield an adequate signal-to-noise ratio ratio (~ 10) in the spectra of the vast majority of the optical candidates ($19 < O < 21$). With this set-up the overall intrumental resolution was 3 Å. The spectra, fluxed with reference to a nearby standard star observed through the same spectrograph set-up, are displayed in Fig. 2. Since a narrow slit was used, this is a relative flux scale; the absolute level is only accurate to $\sim \pm 50$ per cent. The use of the dichroic results is a significantly decreased signal-to-noise ratio in the region around 5400 Å, and occasionally gives rise to a spurious feature (usually a dip) around these wavelengths. In two cases (CRSS1415.1 + 1140 and CRSS2324.7 + 2315) an electronics fault resulted in no data from the red arm. However, the identification and redshift for both objects are secure from the blue arm data alone.

As far as possible, optical candidates in each PSPC field were observed in order of decreasing X-ray flux. This allowed us to incorporate any field for which we had not managed to observe all optical counterparts down to the original flux limit, $S(0.5\text{–}2\ \mathrm{keV}) > 2 \times 10^{-14}$ erg s^{-1} cm^{-2}, in the final survey, simply by imposing a brighter X-ray flux limit (i.e. the flux of the faintest X-ray source for which we observed the optical counterpart) for that field. This was the case for nine PSPC fields. Based on the observing priority during the run (i.e. the candidates in the longer exposure PSPC fields were identified first) these nine fields are mostly the shorter exposure PSPC fields in the survey.

2.4 Optical identifications

As can be seen from fig. 1(a) in Paper I, a significant number of optical images (~ 35 per cent) identified within 20 arcsec will be chance coincidences, giving rise to multiple optical counterparts for some X-ray sources. For sources with more than one optical counterpart, optical spectroscopy was carried out in order of increasing separation between the X-ray position and optical counterpart until a plausible candidate (e.g. QSO, bright star, emission-line M star) was identified or we coud be certain that we had the correct identification (i.e. two or more galaxies in a cluster). There was only one exception to this rule, CRSS1706.4 + 6042, where a blue stellar object lying 14 arcsec from the X-ray source position was observed in preference to two fainter red stellar objects lying closer to the X-ray position. The identification of this object as a QSO confirmed that we had made the correct decision in this case. At the photographic plate limit, the a priori probability of identifying a QSO by chance in an error circle of 20-arcsec radius is less than 0.01, based on a QSO surface density of 80 deg^{-2} at this magnitude (Boyle, Jones & Shanks 1991), and so we adopted this object as the 'true' optical counterpart of the X-ray source. Similarly, the surface density of bright ($R < 15$) stars at high Galactic latitudes is only ~ 100 deg^{-2} (based on the star count models of Bahcall & Soniera 1980), resulting in a similarly low a priori probability of a chance coincidence.

In total, spectroscopic identifications for 118 optical candidates were obtained, including four objects with X-ray fluxes fainter than our final completeness limit and a further four objects (three QSOs and one BL Lac) which had previously been identified. The observations resulted in an identification for 108 of the 123 X-ray sources in the CRSS. These optical identifications are listed in Table 2. We found that the closest optical counterpart was not the correct identification in only three cases (two QSOs and one NLXG) and a further three cases required observations of additional objects to confirm the identification. Each individual case of a multiple optical identification is discussed in the footnotes to Table 2. The optical spectra of all the true counterparts to the X-ray sources (excluding the NLXGs, which were published in Paper I) identified on the basis of their WHT spectra are plotted in Fig. 2.

Table 3 summarizes the source identification by object type. Of the 15 X-ray sources with no spectroscopic identification, two are bright stars ($O < 12$ mag) and we can assume these to be Galactic stars with a high degree of confidence. A further 11 X-ray sources had no optical counterpart within 20 arcsec of the X-ray position on the POSS. Of the remaining two sources, the optical counterpart to the X-ray source CRSS1416.2 + 1136 had an inconclusive, low signal-to-noise ratio spectrum and the counterparts to the X-ray source CRSS1407.8 + 2833 were not observed owing to lack of time. A further object, CRSS1416.3 + 1137, was tentatively identified as a BL Lac based on the lack of any strong ($W_\lambda > 5$ Å) emission or absorption lines in the optical spectrum. This equivalent-width limit was also used by Stocke et al. (1991) to identify candidate BL Lacs in the EMSS.

A Kolmogorov–Smirnov (KS) test performed on the X-ray flux distribution of both the identified and unidentified sources (i.e. all those with no reliable spectroscopic identification, but excluding the two X-ray sources with bright stellar counterparts) revealed no significant differences between the flux distributions for the two samples at the 95 per cent confidence level. This implies that the incompleteness in the survey is independent of the X-ray flux level. Assuming the two bright stellar objects to be Galactic stars, we obtain a 'spectroscopic' completeness of 89 per cent for the survey. To account for this incompleteness in the analysis below we have therefore multiplied the total areas surveyed at each X-ray flux limit by 0.89 to yield effective survey areas. The area coverage of the survey can thus be derived straightforwardly from the field flux limits listed in Table 1. We note that in a few cases (up to three) it is

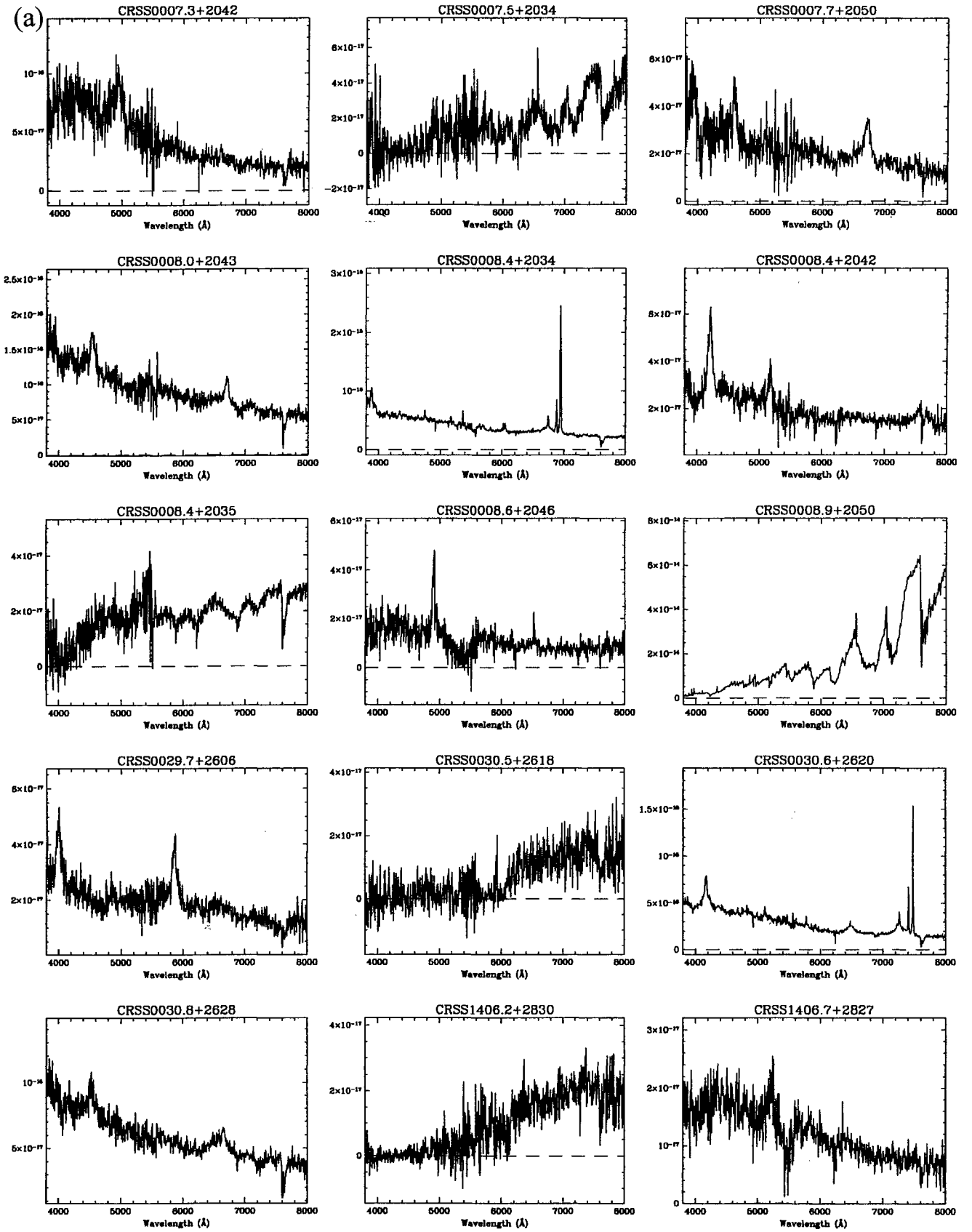

Figure 2. Optical spectra of the CRSS sources (excluding NLXGs) extending from 3800–8000 Å at a resolution of 3 Å pixel^{-1} in units of F_λ erg cm^{-2} s^{-1} Å^{-1}.

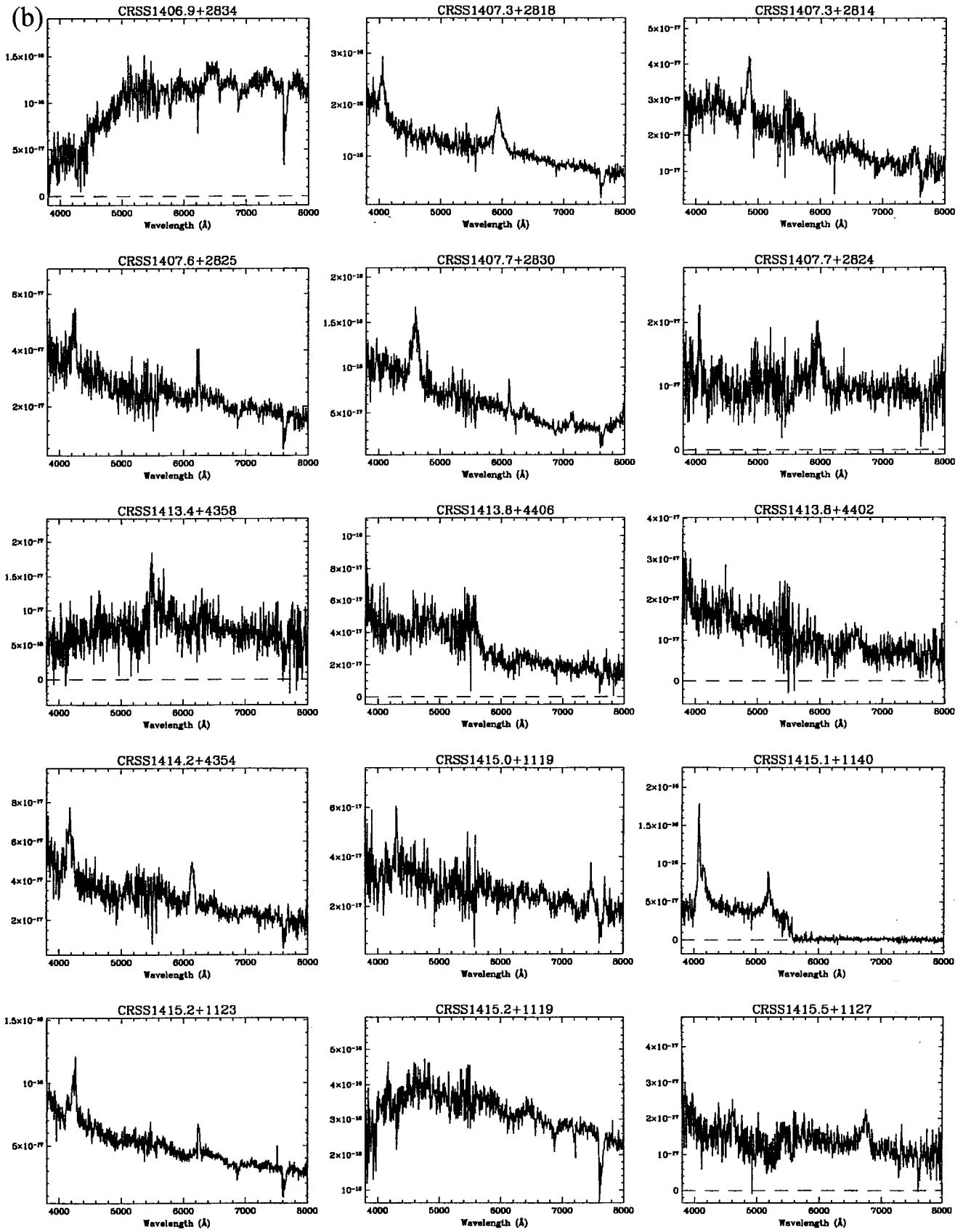

Figure 2 – *continued*

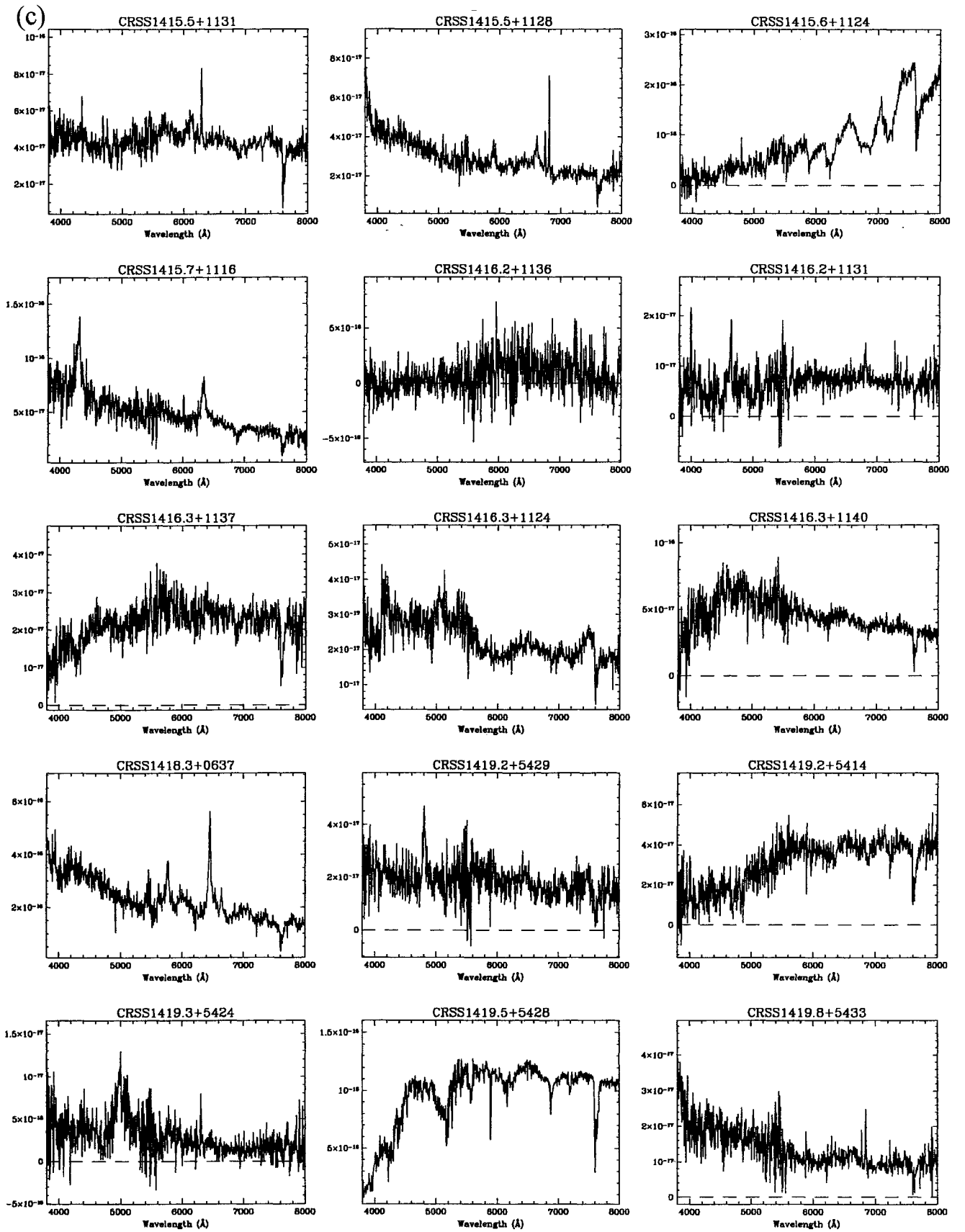

Figure 2 – *continued*

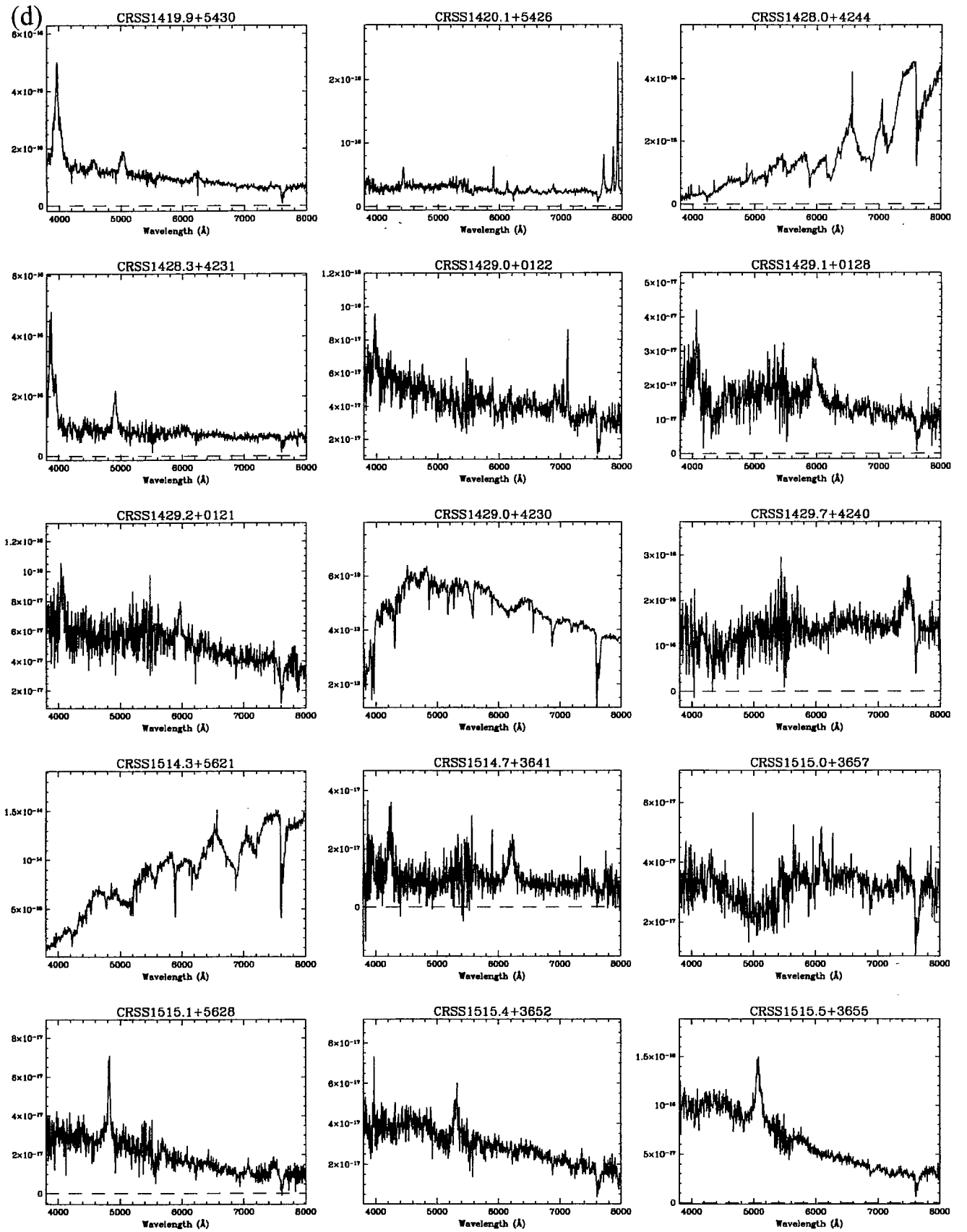

Figure 2 – *continued*

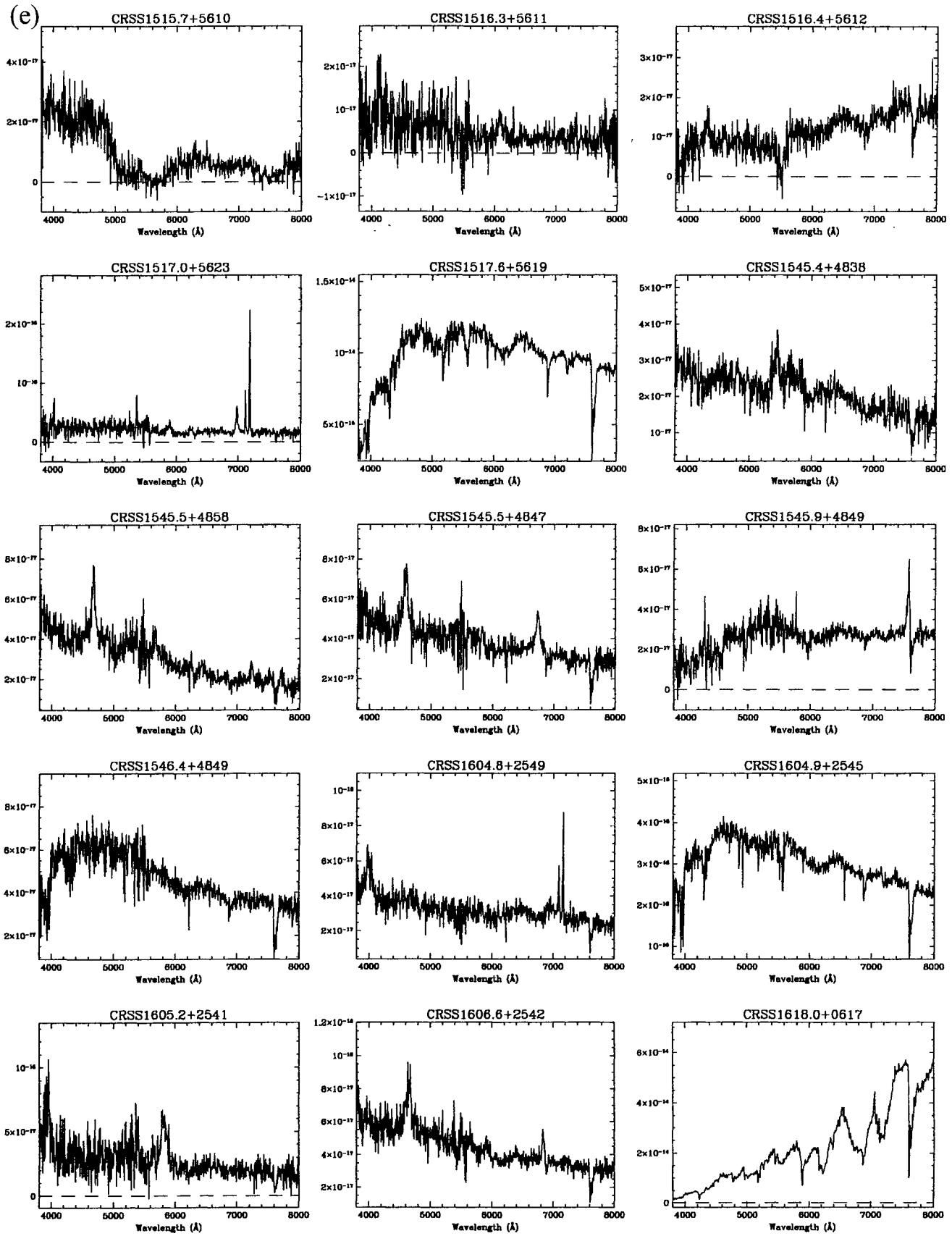

Figure 2 – *continued*

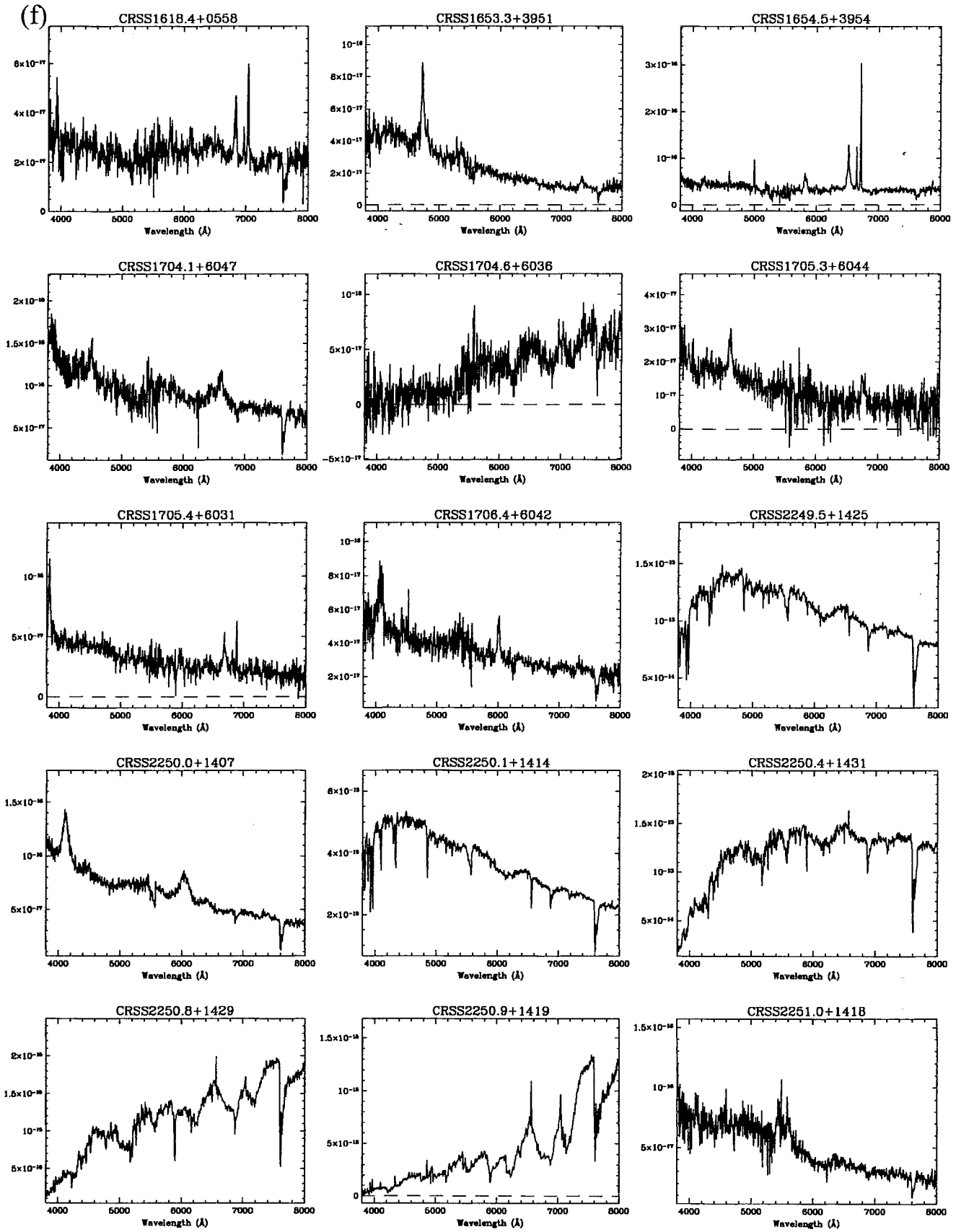

Figure 2 – *continued*

Opposite p. 522, MNRAS, **285**

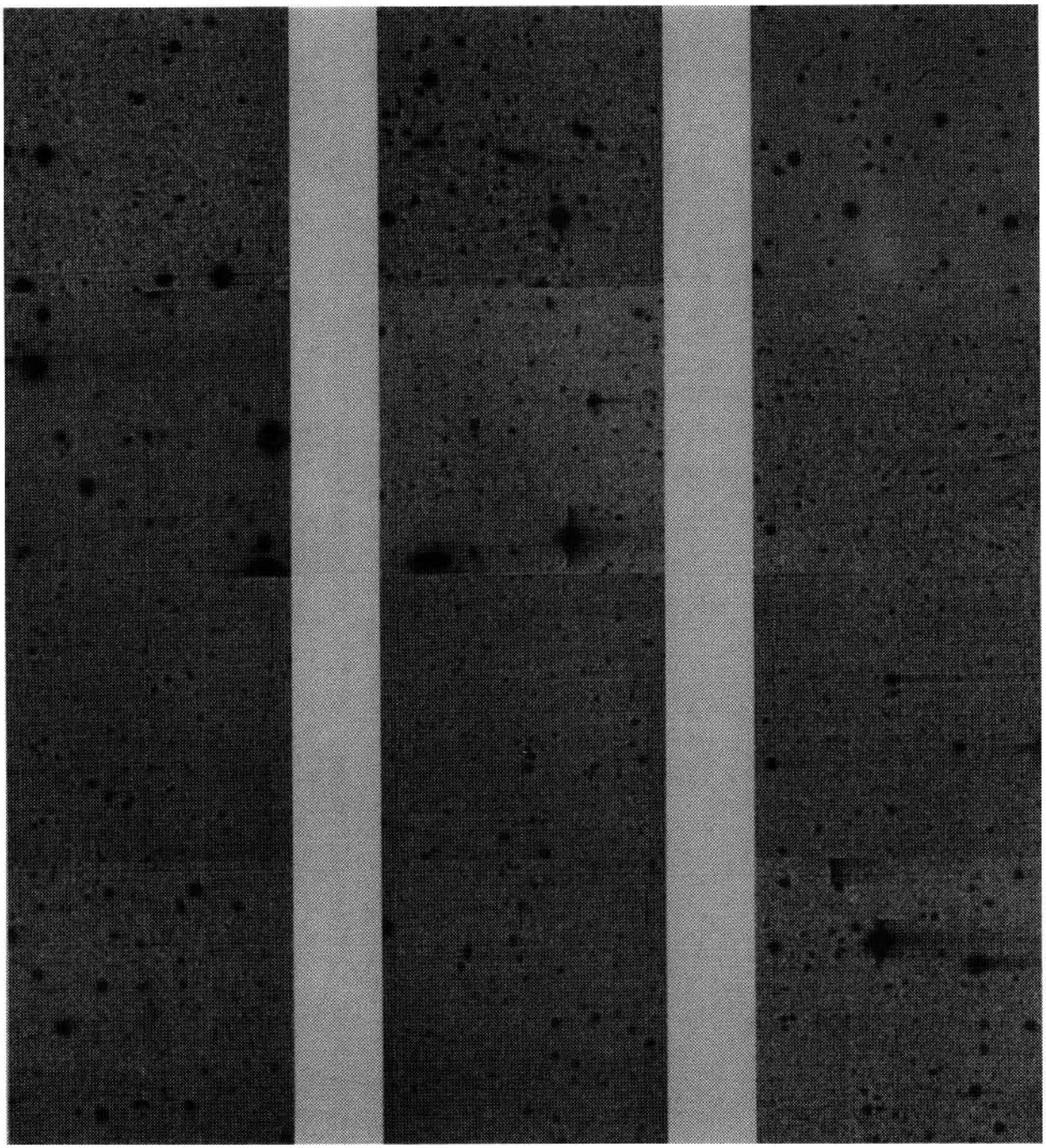

Figure 3. The CCD images for each of the POSS 'blank' fields and the $z = 0.52$ galaxy cluster field. In each frame a 3×3 arcmin^2 region centred on the X-ray source position is shown. North is up and east is to the left. Top row (left to right): CRSS0029.1 + 2616, CRSS0030.5 + 2618 ($z = 0.52$ cluster) and CRSS1413.0 + 4406; second row: CRSS1413.9 + 4352, CRSS1415.3 + 1137 and CRSS1415.6 + 1127; third row: CRSS1415.9 + 1139, CRSS1416.0 + 1142 and CRSS1416.3 + 1129; bottom row: CRSS1429.1 + 4241, CRSS1516.8 + 5617 and CRSS1605.2 + 2602.

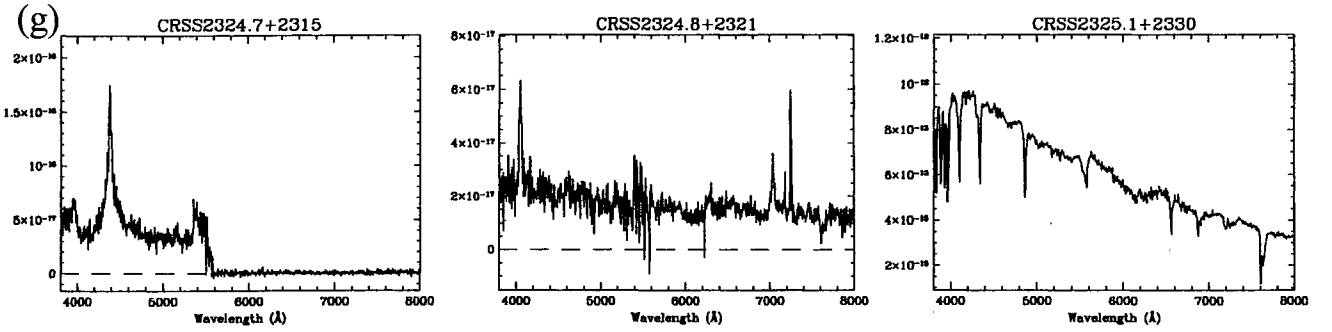

Figure 2 – *continued*

Table 3. Summary of identifications.

Identification	Number
QSO	68
NLXG	12
BL Lac	2
Early Type Galaxy	2
Galaxy Cluster	2
M Star	11
F/G Star	11
No optical counterpart	11
Optical counterpart not observed	3
Inconclusive optical spectrum	1
Total	123

Table 4. CCD galaxy counts.

Source Name	Mean density deg^{-2}	Number in 20 arcsec circle Observed	Predicted
CRSS0029.1+2616	25795	5	2.3
CRSS1413.0+4406	25048	6	2.4
CRSS1413.9+4352	16713	3	1.6
CRSS1415.3+1147	34150	1	3.3
CRSS1415.6+1127	32115	6	3.1
CRSS1415.9+1139	35296	1	3.4
CRSS1416.0+1142	35396	4	3.4
CRSS1416.3+1129	28281	8	2.7
CRSS1429.1+4241	23730	5	2.3
CRSS1516.8+5617	25563	3	2.6
CRSS1605.2+2602	27230	4	2.6
CRSS0030.5+2618†	24621	8	2.5

†Spectroscopically identified as a $z = 0.52$ cluster.

possible that we have identified a relatively faint F or G star which is not the true counterpart of the X-ray source. All such cases are discussed in the footnotes to Table 2. Removing these objects from the sample would reduce the completeness of the survey, but the 'loss' of these objects from the survey is likely to be compensated for by the detection of a similar number of galaxy groups or clusters detected in the 'blank' fields based on CCD imaging (see below).

2.5 CCD imaging

Intermediate-depth (600-s) *R*-band CCD images were obtained with the Isaac Newton Telescope for all of the fields with no optical counterpart on the POSS and one of the X-ray sources identified spectroscopically as a galaxy cluster (CRSS0030.5 + 2618). These observations were carried out as part of the service observation programme on 1994 May 12/13 and on 1995 October 18/19. Observations on 1994 May 12/13 were performed with the EEV CCD and observations on 1995 October 18/19 were carried out with the Tektronix CCD. Both CCDs have a pixel scale of 0.6 arcsec pixel^{-1}. The seeing in both runs ranged from 1.5 to 2.5 arcsec (typically near the lower end of this range). Neither of the two nights was photometric. After bias-subtraction and flat-fielding, we carried out image detection on each CCD frame using the IMAGES routine (see Section 2.1). Images with four or more connected pixels lying more than 2σ above the mean sky-background level were classified as real. Given the rather coarse pixel scale, we made no attempt to perform any classification of stars and galaxies; at the magnitude limit of the CCD frames ($R < 23$) the vast majority of the images (> 90 per cent) will be galaxies. In order to establish the significance of any group or cluster of galaxies seen at the position of the X-ray source on each CCD image, we compared the number of objects found within a 20 arcsec radius circle centred on the X-ray source position to the number expected based on the mean density of objects detected on that CCD frame. The results are presented in Table 4 and a mosaic of the CCD images based on 3×3 arcmin^2 region surrounding each 'blank' field is plotted in Fig. 3, opposite p. 522.

Based on the *R* galaxy counts published by Metcalfe et al. (1991), the mean image surface density on each field is consistent with an *R*-magnitude limit in the range ($22.5 < R < 23.25$). Out of the 11 'blank' fields, four (CRSS0029.1 + 2616, CRSS1413.0 + 4406, CRSS1416.3 + 1129 and CRSS1429.1 + 4241) exhibit a galaxy density twice that of the background and are likely to be galaxy groups or clusters. Although the numbers in any one field are small, the total numbers of images observed within the 20-arcsec radius on the four potential cluster fields is 24, compared with 9.9 expected based on the mean galaxy surface density in the field. This corresponds to a 4.5σ excess based on Poisson statistics. In contrast, we detect only 22 objects on the other seven 'blank' fields compared with 19.9 expected. Individual notes on the CCD images of the 'blank' fields are provided in Table 2.

The possible identification of a further four sources as groups/clusters brings the overall completeness of the CRSS to ~92 per cent. However, we prefer to retain the spectroscopic completeness (~89 per cent) factor in the analysis below, as the galaxy excess observed in these fields has not positively been identified as being the true counterpart to

the X-ray source. Indeed, we can not rule out the possibility that the counterpart to the X-ray source in any of these 'blank' fields is an object with a low optical-to-X-ray flux ratio (e.g. an obscured active galactic nucleus). However, the statistical excess of galaxies identified in these CCD frames argues that at least some of these X-ray sources are associated with galaxy groups or clusters.

We also observed the field of CRSS0030.5 + 2618 which was identified spectroscopically as a $z = 0.52$ galaxy cluster. The CCD image shows a very rich cluster (with a measured density three times that of the mean within the 20-arcsec radius). However, the brightness of the cluster galaxies imaged on the CCD is possibly indicative of a lower redshift than that derived from the spectroscopic observations and further observations are planned to investigate this discrepancy.

3 THE CATALOGUE

3.1 General properties

The majority of the objects identified in the CRSS were QSOs (68, see Table 3), classified from the presence of one or more broad (FWHM > 1000 km s^{-1}) emission lines. A further 12 objects were identified as NLXGs and have been reported on extensively elsewhere (Papers I, II). Of the remaining 30 identifications, there are two early-type galaxies, two galaxy clusters ($z = 0.12$ and $z = 0.52$), two BL Lacs and 24 stars, comprising 11 M stars, 11 F/G stars and the two bright ($O < 12$ mag) stars which were not observed but are likely to be F/G stars. As described above, CCD observations of the fields of those X-ray sources without an optical counterpart on the POSS plate indicate up to a further four galaxy groups or clusters.

3.2 QSOs

3.2.1 Space density

The number–flux, $\log N$–$\log S$, and number–redshift, $n(z)$, relations for the 68 QSOs identified in this survey are plotted in Figs 4(a) and (b) and 5. We also plot in these figures the predicted $\log N$–$\log S$ and $n(z)$ relations based on the cosmological evolution of the X-ray (0.3–3.5 keV) luminosity function derived from fits to the EMSS (Maccacaro et al. 1991) and the deep *ROSAT* survey (Boyle et al. 1994). As demonstrated by Maccacaro et al. (1991) the EMSS yields a slow rate of luminosity evolution [$L_X \propto (1+z)^{k_L}$, $k_L = 2.25 \pm 0.1$], whereas much faster rates are derived from the deep *ROSAT* survey ($k_L = 3.34 \pm 0.1$, Boyle et al. 1994) when a cut-off in the evolution at $z_{max} = 1.79$ is included. We have used the fits provided by Boyle et al. (1993, model J) and Boyle et al. (1994, model S) for the EMSS and deep *ROSAT* samples respectively. Both models assume $q_0 = 0$, $H_0 = 50$ km s^{-1} Mpc^{-1} and $\alpha_E = 1$ in order to maintain consistency with the values adopted previously for these parameters by Maccacaro et al. (1991). This value of α_E is different from the mean value obtained for the CRSS sample ($\alpha_E = 1.3$, Paper IV). However, an increase in the adopted value for α_E would simply translate to an equal increase in the derived value of k_L in both these models. The predicted $n(z)$ relations for all models have been normalized to the total number of QSOs observed in the CRSS. Note that NLXGs are not included in either relation.

The observed $\log N$–$\log S$ relations agree more closely with the predictions of the model derived from the *ROSAT* deep survey (Boyle et al. 1994), confirming the faster rate of X-ray luminosity evolution ($k_L = 3.34 \pm 0.1$, $z_{max} = 1.79$) for QSOs derived in the *ROSAT* energy range. This is apparent in Fig. 4 where the slower rate of X-ray evolution

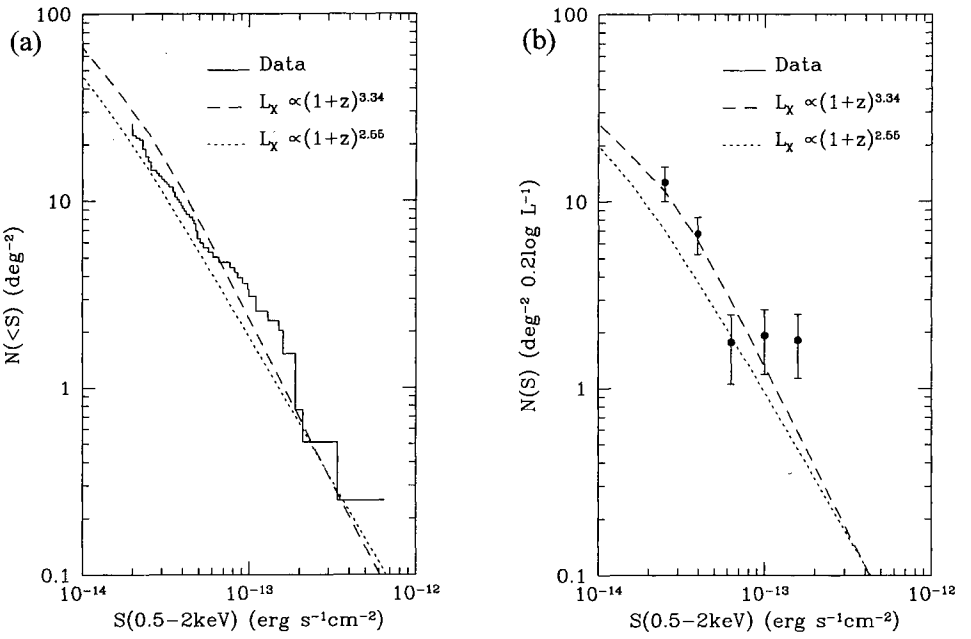

Figure 4. (a) The cumulative number–flux relation for QSOs identified in the CRSS. The predictions of the QSO evolution models described in the text are also plotted. (b) The same data plotted differentially.

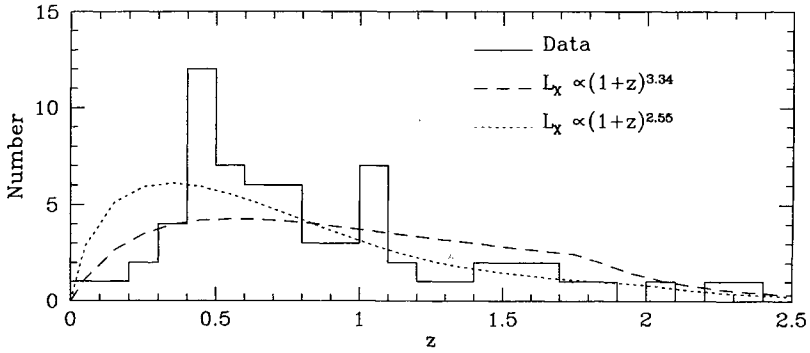

Figure 5. The number–redshift relation for QSOs identified in the CRSS. The predictions of the two QSO evolution models described in the text are also plotted.

($k_L = 2.25 \pm 0.1$) in the *Einstein* data (EMSS, Maccacaro et al. 1991) predicts a lower $\log N$–$\log S$ relation leading to an expected number of QSOs in the CRSS of 41 compared with the 68 observed. The *ROSAT* deep survey model predicts 62. Based on purely Poisson statistics, the EMSS-based model can therefore be ruled out at the 3.3σ level.

In Fig. 5, the EMSS slower rate of evolution results in a predicted $n(z)$ for the CRSS sample which is more heavily weighted towards low redshifts than is observed. Formal comparison of the observed and predicted $n(z)$ distributions using a one-dimensional KS test over the range $0 < z < 3$ concludes that the EMSS prediction is different at greater than the 99 per cent confidence level ($P_{KS} = 0.003$) whereas the *ROSAT* deep survey prediction can not be rejected even at the 95 per cent confidence level ($P_{KS} = 0.082$).

Although the *ROSAT* deep survey prediction is an acceptable fit to the $n(z)$, systematic differences between the model and the data are present in Fig. 5. The *ROSAT* model overpredicts the number of objects at low redshift ($z \lesssim 0.4$) and underpredicts those with $0.4 \lesssim z \lesssim 0.8$. If the seven NLXG in the CRSS which are not positively identified as starburst galaxies are included, the low-redshift disagreement disappears, suggesting that it might be a result of the mis-identification of some QSOs as NLXGs at low redshift.

Recent analyses of QSOs identified in the RIXOS (Page et al. 1996) and UK deep surveys (Jones et al. 1996) have yielded evolutionary rates $k_L = 2.9$, intermediate between the rates discussed here. Both these models also incorporate a redshift cut-off ($1.63 < z_{max} < 1.82$), consistent with that derived by Boyle et al. (1994). However, we note that both these analyses include the EMSS sample with the RIXOS or UK deep sample in the determination of the evolution. This is in contrast to the models discussed above which are based on the analysis of the EMSS and *ROSAT* deep surveys separately.

Note that Boyle et al. (1994) also derive an intermediate evolutionary rate ($k_L = 3.0 \pm 0.1$, $z_{max} = 1.89$) when the EMSS is included with the *ROSAT* sample in the overall fit. Similarly, the best-fitting evolution model to the radio-quiet QSOs in the combined EMSS and CRSS surveys has $k_L = 2.7 \pm 0.1$, with no redshift cut-off (Paper III). This is in good agreement with the fit to the combined RIXOS and EMSS survey derived by Page et al. (1996) ($k_L = 2.66$) for a similar evolution model with no redshift cut-off. It thus appears to be a general feature of these fits that the inclusion of the *Einstein*-selected EMSS slows the evolutionary rate that would otherwise be derived from samples of QSOs based on *ROSAT* surveys alone. It will be interesting to see whether surveys such as the RIXOS (Page et al. 1996) or *ROSAT* deep survey (Jones et al. 1996) confirm this behaviour.

3.2.2 *Emission-line properties*

The broad emission lines for all the QSOs newly discovered in this survey were measured using IRAF. The rest frame equivalent widths and full-width at half maximum (FWHM) are given in Table 5. The redshift is repeated for convenience. Given the generally low quality of the data, no attempt was made to deblend the dominant lines from the weaker features with which they are blended, nor was any deblending of the broad and narrow components of Hβ attempted unless the separation was clear (labelled in Table 5). A local, linear continuum was used in combination with a Gaussian profile fit where appropriate, otherwise the data were measured directly (also indicated in Table 5). The accuracy of the line measurements is estimated at ± 30 per cent. The distributions (mean and dispersion assuming a Gaussian distribution) of equivalent widths and FWHM are given in Table 6. The equivalent widths are similar to those from surveys including those in other wavebands. The numbers for Parkes radio-selected, flat radio spectrum QSOs (Wilkes 1982, 1986; Wilkes et al. 1983) are shown for illustration.

We note a few interesting discrepancies with recent data sets. Although the equivalent width of Hβ agrees well with that of the radio-selected QSOs, its value is approximately half that of the optically selected PG sample (98 ± 37 Å, Boroson & Green 1992). This latter data set has high signal-to-noise (S/N) ratio spectra and a detailed deblending of Hβ from surrounding weak Fe II features was performed. It is possible that the low S/N ratio of the optical spectra of both the radio- and X-ray-selected samples results in the blended Fe II emission systematically raising the apparent continuum level around Hβ and lowering the apparent line strength. Clearly, higher S/N ratio optical data are necessary to investigate this further.

It has been reported that radio-loud QSOs have narrower ultraviolet (UV) lines than radio-quiet QSOs (Brotherton

Table 5. QSO emission-line measurements.

Name	z	Lyα/NV		CIV		CIII]		MgII		Hβ	
		W_{λ_0}	Δv	W_{λ_0}	Δv	W_{λ_0}	Δv	W_{λ_0}	Δv	W_{λ_0}	Δv
0007.3+2042	0.769							47	7.7		
0007.7+2050	1.396			75[a]	6.0	23[a]	4.8	44	5.2		
0008.0+2043	1.381			37	12.0	13	5.1	12	2.9		
0008.4+2034	0.389							39[a]	4.9	19[a]	5.3
0008.4+2042	1.710			35	5.8	11	3.0	25	6.0		
0008.6+2046	0.752							57	2.9	65	2.2
0029.7+2606	1.094					23	5.3	32	4.0		
0030.6+2620	0.493							30	5.4	74	8.1[b]
0030.8+2628	1.372			17[a]	3.9	14[a]	6.9	34	12.2		
1406.7+2827	0.878							25	6.6		
1407.3+2818	1.121					15[a]	4.4	40[a]	5.4		
1407.3+2814	0.728							33	5.6	36	2.6
1407.6+2825	1.222					14	4.8	8[a]	1.7		
1407.7+2830	0.642							57[a]	8.2	65	8.0
1407.7+2824	1.127					22	4.4	17	3.2		
1413.4+4358	0.950							74[a]			
1413.8+4406	0.978					17	4.3	35[a]			
1413.8+4402	1.347			52[a]	6.9	12[a]		59[a]	9		
1414.2+4354	1.197					35	8.3	21[a]	3.2		
1415.0+1119	0.538							12	2.9	40[a]	1.8
1415.1+1140	2.353	55[a]	2.7	8	1.6						
1415.2+1123	1.230			18	5.5	7	1.5				
1415.5+1127	1.412			24	5.5	9	3.5	20	4.5		
1415.5+1131	0.257									14	3.8
1415.5+1128	0.360							15	3.9	20	2.9
1415.7+1140	1.257					20	5.3	17	2.9		
1416.2+1131	1.429					21	2.2	7	2.0		
1416.3+1124	1.673			12[a]		12	7.7	32	9.3		
1418.3+0637	0.329									66[a]	1.7
1418.4+0558	0.406							15	2.4	29	1.6
1419.2+5429	0.722							31	2.9	54	3.0
1419.3+5424	0.785[d]							135[a]	10.0		
1419.8+5433	0.367							18	4.9	23	5.7
1419.9+5430	2.257	53[a]	4.9	14	4.8	8	4.6				
1420.1+5426	0.583							13	1.5	40	1.1
1428.3+4231	2.171	67[a]	4.2	21[a]	3.0	15[a]					
1429.0+0122	0.416							20	4.5	32	6.6
1429.1+0128	1.131							19	4.2		
1429.2+0121	1.127					13	4.5	11	3.2		
1429.7+4240	1.672							33	6.3		
1514.7+3641	1.219					37	4.3	44	4.6		
1515.0+3657	0.253									88[c]	2.2[c]
1515.1+5628	0.723							23	2.1	23	1.2
1515.4+3652	0.893					22[a]	1.6	26	4.5		
1515.5+3655	0.812							40[a]	5.3		
1515.7+5610	0.296									59[c]	1.7[c]
1516.3+5611	1.168					21	3.3	38	4.5		
1517.0+5623	0.434							28	2.4	56	1.5
1545.4+4838	0.937					20[a]		19[a]			
1545.5+4858	0.666							28	3.9	29	2.1
1545.5+4847	1.403					25	6.5	11	3.8		
1545.9+4849	0.154										
1604.8+2549	0.426							24	7.3	33	7.4
1605.2+2541	1.071					48[a]		61	5.5		
1606.6+2542	1.436			28	5.3	13	5.1	7	1.7		
1653.3+3951	0.692							50[a]	2.8	46[a]	3.2
1654.5+3954	0.340							44	2.2	61	1.0
1704.1+6031	1.362			25	3.9	5	2.9	8	3.3		
1705.4+6031	0.375							20	2.5	40	2.6
1705.3+6044	1.416			37	4.4	12	3.3	22[a]			
1706.4+6042	1.142					22	6.6	14	2.1		
2250.0+1407	1.159					19	7.4	28	8.2		
2251.0+1418	0.962					18	5.4	39	12		
2324.7+2315	1.828			51	3.2						
2324.8+2321	0.447							40	2.7	33	1.4

Notes.
Rest equivalent with (W_{λ_0}) is given in Å. Rest FWHM (Δv) is given in units of 10^3 km s^{-1}. [a]Gaussian fit inappropriate/impossible for this line. [b]Hβ broad component only. [c]Hα measurements. [d]In the absence of C IV, the single line is identified as Mg II. Its high equivalent width suggests an ID of Lyα with $z=3.108$, although the proximity of the emission line to the dichroic cut-off could also be a factor.

Table 6. Distribution of emission-line measurements.

	W_{λ_0} (Å)			FWHM/10^3 km s^{-1}		
Line	Mean	σ	No.	Mean	σ	No.
CIV	30(32)	18	15	5.1(5.0)	2.4	14
CIII]	18(17)	9	32	4.8(5.8)	1.8	28
MgII	29(27)	16	53	4.7(4.3)	2.6	50
Hβ	41(47)	18	21	3.4(4.8)	2.4	21

Note: the numbers in brackets are for Parkes flat-spectrum radio-selected QSOs.

et al. 1994; Baldwin, Wampler & Gaskell 1989; Francis, Hooper & Impey 1993), a difference which has been interpreted in terms of differing structure and line ratios in the emitting region. This difference is most notable for the C III] λ1909 line owing to it blending with Al III λ1858. In the current X-ray-selected, predominantly radio-quiet (Paper III) sample, the FWHM of the C III] blend agrees with that of the radio-loud (5000–6000 km s^{-1}) rather than the radio-quiet (7000–9000 km s^{-1}) QSOs in these earlier papers. This implies that X-ray emission is a factor in determining the UV emission-line widths such that X-ray selection results in a systematically different (narrower emission-line) subset of the radio-quiet QSO population than optical selection. The correlation between optical-to-X-ray flux ratio and the X-ray spectral index present in the optically selected sample of Laor et al. (1996) predicts the opposite effect since in their sample the X-ray-loud objects have broader lines. Clearly, confirmation and a definitive interpretation of these results must await a detailed investigation using higher quality optical spectra.

The strongest correlation reported by Laor et al. (1994, 1996) is an inverse relation between the FWHM(Hβ) and the soft X-ray slope for their sample of low-redshift PG QSOs. In addition, Boller, Brandt & Fink (1996) report a strong tendency for QSOs with narrower lines to have much steeper (softer) X-ray spectra. We tested for such a relation in our sample using the X-ray slopes reported in Paper IV, but found none. We also found no relation between the X-ray slope and the FWHM for C IV λ1549, C III] λ1909 or Mg II λ2798 (see Fig. 6). Notably, our sample was selected in the *ROSAT* hard band (0.5–2 keV) and so is biased against the unusually soft sources reported by Boller et al. (1996) and includes a significantly smaller range of X-ray slopes than the optically selected sample ($\Delta\alpha_E \sim 1$ cf. $\Delta\alpha_E \sim 2$ of Laor et al. 1996). It seems likely that the different selection criteria combined with the smaller distribution of X-ray slopes combine to mask any correlation in our sample.

4 CONCLUSIONS

Here we summarize the conclusions of all five papers in this series. Our spectroscopic survey of 123 sources detected in a medium-depth *ROSAT* survey [$S(0.5\text{–}2\ \mathrm{keV}) > 2 \times 10^{-14}$ erg s^{-1} cm^{-2}] has yielded new identifications for 108 objects; including 68 QSOs, 12 narrow-emission-line X-ray galaxies, 22 stars, two BL Lac objects, two galaxies and two clusters. In addition, two X-ray sources are coincident with bright stars and deep CCD imaging reveals tentative evidence for faint galaxy groups/clusters at the positions of a further four sources. In total, a possible identification exists for up to 92 per cent of the sources in the CRSS. In this paper we have shown that the number–flux and number–redshift relations for QSOs identified in this survey are consistent with the fast rate of cosmological luminosity evolution previously derived from deep *ROSAT* surveys [$L_X \propto (1+z)^{3.34 \pm 0.1}$]. The emission-line equivalent-width distribution for the X-ray QSOs identified in this survey is similar to those determined from surveys at other wavelengths. The line widths, specifically that of the C III] blend, are more similar to radio-loud than optically selected, radio-quiet objects implying that X-ray selection affects the emission-line properties of the sample. We do not confirm an inverse correlation between the emission-line width and the X-ray spectral slope, which is probably because of the different selection and properties of the comparative samples.

The NLXGs in both the current and EMSS samples, discussed in Papers I and II, comprise a roughly equal mix of AGNs and starburst galaxies as distinguished by their optical emission-line ratios. Their X-ray evolution and X-ray spectral properties (see also Paper IV) are indistinguish-

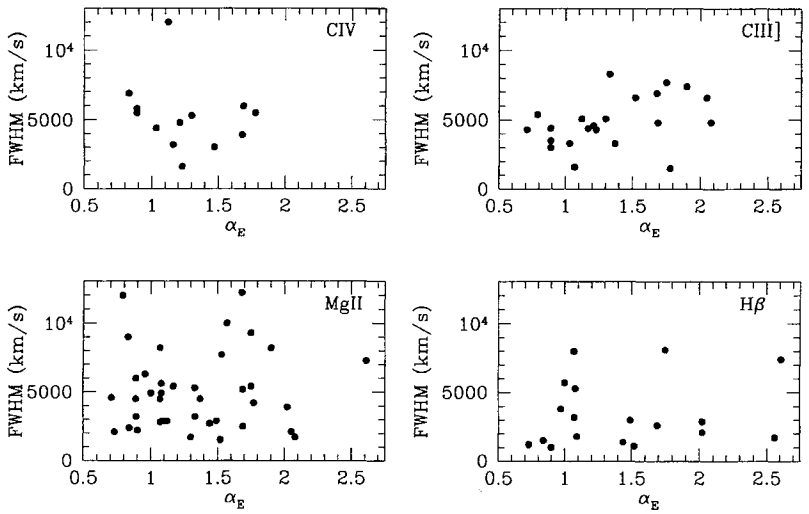

Figure 6. Widths of the prominent emission-line blends as a function of the *ROSAT* X-ray spectral slope.

able from one another and from those of QSOs. We estimate that the two classes contribute approximately equally to the X-ray background at a level of ~ 10 per cent (Papers I, II).

The X-ray luminosity function for radio-loud and radio-quiet QSOs in the combined CRSS and EMSS sample shows that, while the luminosity evolution is similar in the two classes, the shape of the de-evolved luminosity function is different (Paper III). This difference can be explained in terms of the additional, beamed, radio-linked X-ray component, commonly believed to be present in radio-loud QSOs (e.g. Zamorani et al. 1981, Wilkes & Elvis 1987, Shastri et al. 1993).

A detailed analysis of the X-ray spectral properties of QSOs and NLXGs over the full 0.1–2.4 keV energy range of the *ROSAT* PSPC (Paper IV) demonstrates that a single power-law slope with Galactic absorbing column density yields a good fit for the majority of sources. The mean slope for the QSOs is 1.3 with a dispersion of 0.5 and no redshift dependence. The most probable explanation of this latter result is that these QSOs exhibit a single-power-law X-ray spectrum from 0.1–7.3 keV with no change in slope. In contrast, the CRSS NLXGs do show evidence for a decrease in their spectral slope with redshift.

ACKNOWLEDGMENTS

BJB acknowledges the receipt of a Royal Society University Research Fellowship and the support and hospitality of the Smithsonian Astrophysical Observatory. The X-ray data were obtained from the Leicester and Goddard *ROSAT* archives. This work was partially supported by NASA grants NAGW-2201 (LTSA) and NAG5-3066 (ADP) and NASA contracts NAS5-30934 (RSDC) and NAS8-39073 (ASC). The optical spectra were obtained at the William Herschel Telescope at the Observatory of the Roque de los Muchachos operated by the Royal Greenwich Observatory.

REFERENCES

Bahcall J. N., Soniera R., 1980, ApJS, 44, 73
Baldwin J. A., Wampler E. J., Gaskell C. M., 1989, ApJ, 338, 630
Boller T., Brandt W. N., Fink H. H., 1996, A&A, 305, 53
Boroson T. A., Green R. F., 1992, ApJS, 80, 109
Boyle B. J., Jones L. R., Shanks T., 1991, MNRAS, 251, 482
Boyle B. J., Griffiths R. E., Shanks T., Stewart G. C., Georgantopoulos I., 1993, MNRAS, 260, 49
Boyle B. J., Shanks T., Georgantopoulos I. G., Stewart G. C., Griffiths R. E., 1994, MNRAS, 271, 639
Boyle B. J., McMahon R. G., Wilkes B. J., Elvis M., 1995a, MNRAS, 272, 462 (Paper I)
Boyle B. J., McMahon R. G., Wilkes B. J., Elvis M., 1995b, MNRAS, 276, 315 (Paper II)
Branduardi-Raymont G. et al., 1994, MNRAS, 270, 497
Brotherton M. S., Wills B. J., Steidel C. C., Sargent W. L. W., 1994, ApJ, 423, 131
Ciliegi P., Elvis M., Wilkes B. J., Boyle B. J., McMahon R. G., Maccacaro T., 1995, MNRAS, 277, 1463 (Paper III)
Ciliegi P., Elvis M., Wilkes B. J., Boyle B. J., McMahon R. G., Maccacaro T., 1997, MNRAS, 284, 401 (Paper IV)
Crampton D., Cowley A. P., Hartwick F. D. A., 1987, ApJ, 268, 565
Francis P. J., Hooper E. J., Impey C. D., 1993, AJ, 106, 417
Gioia I. M., Maccacaro T., Schild R. E., Wolter A., Stocke J. T., Morris S. L., Henry J. P., 1990, ApJS, 72, 567
Irwin M. J., Maddox S. J., McMahon R. G., 1994, Spectrum, 2, 14
Jones L. R. et al., 1996, in Zimmermann H. U., Trümper J. E., Yorke H., eds, MPE Report 263, Röntgenstrahlung from the Universe. Max-Planck-Institut für Extraterrestrische Physik, Garching, p. 457
Hasinger G., Burg R., Giacconi R., Hartner G., Schmidt M., Trümper J., Zamorani G., 1993, A&A, 275, 12
Maccacaro T., Dela Ceca R., Gioia I. M., Morris S. L., Stocke J. T., Wolter A., 1991, ApJ, 274, 117
Metcalfe N., Shanks T., Fong R., Jones L. R., 1991, MNRAS, 249, 498
McMahon R. G., 1991, in Crampton D., ed., ASP Conf. Ser. 21, The Space Distribution of Quasars. Astron. Soc. Pac., San Francisco, p. 129
Laor A., Fiore F., Elvis M., Wilkes B., McDowell J., 1994, ApJ, 435, 611
Laor A., Fiore F., Elvis M., Wilkes B., McDowell J., 1997, ApJ, in press
Page M. J., Carerra F. J., Mittaz J. P. D., Mason K. O., Hasinger G., 1996, in Simmermann H. U., Trümper J. E., Yorke H., eds, MPE Report 263, Röntgenstrahlung from the Universe. Max-Planck-Institut für Extraterrestrische Physik, Garching, p. 497
Schmidt M., Green R. F., 1983, ApJ, 269, 352
Shanks T., Georgantopoulos I., Stewart G. C., Pounds K. A., Boyle B. J., Griffiths R. E., 1991, Nat, 353, 315
Stocke J. T., Morris S. L., Gioia I. M., Maccacaro T., Schild R., Wolter A., Fleming T. A., Henry J. P., 1991, ApJS, 76, 813
Shastri P., Wilkes B. J., Elvis M., McDowell J. C., 1993, ApJ, 410, 29
Wilkes B. J., 1986, MNRAS, 218, 331
Wilkes B. J., 1982, PhD thesis, Univ. Cambridge
Wilkes B. J., Elvis M., 1987, ApJ, 323, 243
Wilkes B. J., Wright A. E., Jauncey D. L., Peterson B. A., 1983, Proc. ASA, 4, 3
Zamorani G. et al., 1981, ApJ, 245, 357